

Table of Contents

1. Abstract.....	1
2. List of Abbreviations Used.....	2
3. Introduction.....	4
4. Background.....	10
4.1 Anatomy relevant to B-line formation.....	10
4.2 The importance of artifact analysis in LUS.....	12
4.3 Definition of important artifacts in LUS.....	13
4.4 Definition and characteristics of B-lines.....	14
4.5 Disambiguation of B-line terminology.....	15
4.6 Clinical significance of B-lines in various conditions.....	17
4.7 Expanding the suite of features.....	19
4.8 Challenges in analyzing B-lines.....	20
4.9 Physics of Lamb Waves.....	21
5. Literature-Review.....	22
5.1 Theories of B-line Formation.....	22
5.2 Models for B-line Generation.....	26
6. Methodology.....	29
6.1 Wrapped Sponge.....	29
6.2 Membrane Vice.....	32
6.3 Pith Pits.....	35
6.4 Digital Simulations.....	38
7. Results.....	39
7.1 Wrapped Sponge.....	39
7.2 Membrane Vice.....	40
7.3 Pith Pits.....	41
7.4 Digital Simulation.....	42
8. Discussion.....	44
9. Conclusions.....	48
10. Bibliography.....	50

1. Abstract

As a consequence of the particular needs of the COVID-19 pandemic, Lung Ultrasound has gained wider acceptance as a valuable diagnostic tool. Previously, there was persistent resistance to Lung Ultrasound, despite its meaningful benefits in safety, cost and speed, that stemmed from its reliance on artifact analysis. In other situations, artifacts are undesired byproducts of the imaging system, but key artifacts, such as the B-lines, are central to Lung Ultrasound interpretation. The distinctive B-line vertical artifact is associated with various pulmonary pathologies. While B-lines are widely used clinically, their formation mechanism remains incompletely understood.

Most theories of B-line generation focus on parenchymal explanations and neglect the potential role of the pleural membrane. This research investigates the contribution of the pleural membrane to B-line formation to fill this gap in the scientific literature. In this work it is hypothesized that minor geometric changes to the pleural surface can provide loci for ultrasonic energy re-emission, and that the pleural membrane may prolong B-line signals through the gradual conveyance of Lamb waves to these loci. To test these hypotheses, three experimental models were developed: a Wrapped Sponge model, a Membrane Vice model, and a Pith Pit model. Digital simulations using LS-DYNA software complemented the physical experiments.

The Wrapped Sponge model produced short vertical artifacts that increased with water content. Unexpectedly, long vertical artifacts resembling B-lines were observed at the phantom edges where loose membrane folds contacted the gel spacer. The Membrane Vice model further isolated the pleural membrane's role. It demonstrated that simple concave V-shaped folds in a membrane could consistently produce long vertical artifacts reminiscent of B-lines. Material properties of the membrane significantly influenced artifact formation, with plastic wrap and sausage casing producing strong artifacts while vinyl rubber did not. Conversely, the Pith Pit model, lacking a membrane, produced only short artifacts. The digital simulations provided additional support for the proposed theory, demonstrating the feasibility of surface waves to propagate along the lung surface at speeds sufficient to resupply energy to B-line origin sites.

These findings suggest a "pleura-genic" mechanism for B-line formation, complementing traditional "parenchyma-genic" explanations. This novel perspective may help explain clinical observations such as the erasure of A-lines in the presence of B-lines and the occurrence of B-lines in conditions without excess lung fluid. The study implies that B-line characteristics could potentially provide information about pleural properties, opening new possibilities for Lung Ultrasound application.

2. List of Abbreviations Used

A-mode: Amplitude mode - A single ultrasound scan line displaying echo amplitude vs. depth.

ARDS: Acute Respiratory Distress Syndrome - A severe lung condition characterized by difficulty of breathing and fluid in the lungs.

B-mode: Brightness mode - The most common ultrasound imaging mode, displaying a 2D grayscale image.

CAD: Computer-Aided Design - Used for part design and rapid prototyping.

COPD: Chronic Obstructive Pulmonary Disease - A lung disease causing airflow blockage and long-term breathing problems.

CPE: Cardiogenic Pulmonary Edema - Fluid accumulation in the lungs due to heart problems.

CT: Computed Tomography - An X-ray imaging technique producing cross-sectional images of the body.

DAH: Diffuse Alveolar Hemorrhage - A condition involving bleeding into the lungs' air sacs.

FEM: Finite Element Method - A numerical technique for solving complex engineering problems where an analytical solution would be too difficult.

GGO: Ground Glass Opacity - A hazy area on CT scans indicating partial loss of aeration in the lungs.

LDZ: Lung Disease Zone - An area of the lung affected by disease or abnormality.

LUS: Lung Ultrasound - The use of ultrasound imaging to examine the lungs and pleural space.

MI: Mechanical Index - A measure of the strength of ultrasound pulses used to gauge the potential for ultrasound-induced bioeffects and cavitation.

M-mode: Motion mode - An ultrasound imaging mode that displays movement of structures over time.

MRI: Magnetic Resonance Imaging - An imaging modality that uses the reaction of different concentrations of hydrogen atoms in strong magnetic fields to create contrast.

NDE: Non-Destructive Examination - The industrial application of ultrasound technologies for testing methods that do not damage the material being inspected.

POCUS: Point of Care Ultrasound - Ultrasound performed and interpreted by the clinician at the patient's bedside.

PMMA: Poly(methyl methacrylate) - Also known as acrylic or Perspex, used in the construction of the membrane vice.

PVC: Polyvinyl Chloride - A synthetic plastic polymer used in various applications, including medical devices.

RF: Radio Frequency - High-frequency raw data from the transducer.

RT-PCR: Reverse Transcription Polymerase Chain Reaction - A molecular test that serves as the gold standard for COVID-19 diagnosis.

SARS-CoV-2: Severe Acute Respiratory Syndrome Coronavirus 2 - The virus responsible for the COVID-19 pandemic.

SNR: Signal-to-Noise Ratio - Measure of how much statistical noise is in an image, allowing for cross platform comparisons of image quality.

TGC: Time Gain Compensation - It is the mathematical correction applied to later returning ultrasound echoes which allows for relative strength comparisons between them by making up for the additional attenuation losses the waves underwent before arriving.

US: Ultrasound - An imaging modality and the frequency domain for mechanical waves above that of human hearing.

3. Introduction

The ability to visualize the human body's internal structures and workings has not always been available to physicians. The evolution of medical imaging has marched along with the advancement in other technological arenas, opening new avenues to examine patients. Ultrasound was first used for medical imaging in the mid-20th century by Ian Donald. Since then, ultrasound has revolutionized fields such as Gynecology [Harrison, 2003] and Cardiology [Herbst, 2024]. However, despite being a highly versatile and non-invasive imaging modality, for decades ultrasound was not commonly utilized to examine the lungs due to the lungs' air-filled nature because it was thought that this represented an insurmountable barrier [Weinberger, 2005].

Slowly this perception began to change. Although in aerated lungs it is still not possible to obtain structural information, researchers and clinicians started to discover applications for US in lung evaluation as they began to recognize distinctive ultrasound artifacts in lung imaging, particularly the B-line artifact. Gradually, LUS was becoming more accepted for monitoring patients at their bedside [Lichtenstein, 2014], but until the outbreak of COVID19 it was still niche [Demi, 2022b].

With the arrival of SARS-CoV-2 and the ensuing pandemic, came a seismic shift in the field [Vetrugno, 2020]. As the medical community struggled to handle the chaos unleashed by the spread of the Severe Acute Respiratory Syndrome COronaVirus 2 (SARS-CoV-2) virus, Lung Ultrasound (LUS) became a favored tool to manage the large number of cases. The global pandemic and flood of COVID19 pneumonia cases highlighted the various advantages of the long undervalued clinical techniques of LUS and catalyzed its more widespread adoption [Demi, 2022b] [Vetrugno, 2020]. Soon many clinicians began adopting protocols for LUS to help deal with the flood of new patients [Soldati, 2020].

While its potential has been recognized among researchers for decades, the adoption of LUS had been stymied by its reliance on artifacts over the nearly absent structural information in lung scans. Since the main structure of the lung still remains out of sight under ultrasonic inspection, an analysis of the artifacts present in lung scans are required to determine the state of the lungs [Marini, 2021]. Nevertheless, the methods developed to diagnose and risk-stratify patients with COVID19 plainly demonstrated the real usefulness of artifactual analysis along with the considerable advantages of LUS. Central to LUS interpretation are B-lines, distinctive long hyperechoic vertical artifacts associated with various pulmonary pathologies. During the COVID-19 pandemic, the presence and quantity of B-lines became crucial indicators of disease severity and progression. The newfound popularity of this technique necessitates a greater

understanding of B-line artifacts and their origin, particularly as LUS continues to play an increasingly important role in clinical practice.

However, the lung scoring protocol currently employed in clinical practice [Soldati, 2020] primarily relies on a simple counting of B-lines, potentially overlooking a wealth of additional diagnostic information. This limitation stems from an incomplete understanding of B-line formation mechanisms. While it is known that B-lines originate at the pleural line, most theories focus on parenchymal explanations [Avruch, 1985] [Lichtenstein, 1997] and [Soldati, 2009], neglecting the potential role of the pleura itself.

This research aims to address this gap in the scientific literature by investigating the pleural membrane's contribution to B-line formation. In this work, it is hypothesized that minor geometric changes to the pleural surface can provide a locus where ultrasonic energy imparted to the membrane during the scan can be re-emitted, and further that the pleural membrane may prolong B-line signals through the gradual conveyance of "Lamb" surface waves [Rose, 2014] to these loci. To test these ideas, a simple physical model was developed to represent the air-fluid interface at the lung surface. This model demonstrated that vertical artifacts can in fact be formed in the absence of simulated parenchymal tissue requiring only a membrane for their formation.

Understanding the pleural membrane's role in B-line formation could significantly enhance the diagnostic capabilities of LUS. The thesis that follows will extend the understanding of B-line formation, by addressing the paucity of pleural explanations for B-line formation and unlock new dimensions of potential diagnostic information encoded in B-lines.

Medical ultrasound images are formed by the propagation and reflection of high-frequency sound waves through biological tissues. These waves, typically in the range of 1-20 MHz, are produced by exciting oscillations in piezoelectric crystals within the transducer [Azhari, 2020].

In a transducer waves are created either by a single crystal or by an array of crystals with time delays to form a single focused beam. When the transducer is placed on the skin, pressure waves are sent into the body, causing tissues to alternate between states of compression and rarefaction. The propagation speed of these ultrasound waves in soft tissue is approximately 1540 m/s very close to that of water. At interfaces between tissues with different acoustic impedances, partial reflection occurs according to the equation:

$$(Eq. 1) \quad R = \frac{(Z_2 - Z_1)^2}{(Z_2 + Z_1)^2}$$

where R is the reflection coefficient of intensity, and Z1 and Z2 are the acoustic impedances of the two tissues [Azhari, 2020]. At an air-water interface this results in 99.99% of the energy being reflected.

The choice of frequency is crucial: higher frequencies (shorter wavelengths) improve axial resolution but cannot be indefinitely increased since they attenuate more quickly in tissue, reducing the potential imaging depth. The attenuation coefficient α , describes the decay of the wave over the distance it travels. In soft tissues the attenuation increases approximately proportional to the frequency [Azhari, 2020].

$$(Eq. 2) \quad \alpha(f) = \alpha_0 |f|^b$$

Where f is the frequency, α_0 is the original amplitude and b is a tissue specific parameter that is roughly one for soft tissue.

Once pressure waves return, they deform the piezoelectric crystals of the transducer and the ensuing changes in voltage are recorded. The returning echoes are processed and from their strengths and return times one scan line is made. Echoes that return later are interpreted as being from a source further from the transducer. An important part of the ultrasound data processing occurs before the strength of echoes can be compared. The strength of later echoes are increased in a process called time-gain compensation (TGC) in order to reflect the extra attenuation those signals would have experienced on their journey through the tissue.

Ultrasound imaging can be performed in several modes, each offering unique advantages for specific diagnostic applications. The three primary modes are A-mode, B-mode, and M-mode.

A-mode (Amplitude mode): This is the earliest and most basic form of ultrasound imaging. Following the process outlined in the section above, it produces a single scanline representing a one-dimensional chain of reflected echoes. The amplitude of the reflected signal is displayed as a function of depth. A-mode serves as the foundation for more advanced imaging techniques but is rarely used in clinical practice [Azhari, 2020].

B-mode (Brightness mode): B-mode is the type of US imaging most familiar to the public as it is the most commonly used mode in diagnostic ultrasound. Most lung ultrasound is done in B-mode. To make a B-mode image multiple adjacent scanlines are combined to create a two-dimensional cross-sectional image of the anatomy. Many images can be gathered in succession to display a video. B-mode allows for real-time visualization of anatomical structures. B-lines in LUS are only seen in B-mode but there is no connection between their names.

M-mode (Motion mode): This mode displays the motion of structures over time. Images in M-mode are made by collecting many scanlines in the same location and displaying the data with depth on the vertical axis and time on the horizontal axis. In LUS, it is used to identify the "seashore sign" in normal lungs with healthy lung sliding and the "lung pulse" in unhealthy patients with complete atelectasis that lack lung sliding [Lichtenstein, 2003].

Doppler mode: Doppler is less commonly used in LUS, but it is worth mentioning for completeness. It utilizes the Doppler effect to measure and visualize blood flow. Flow can be detected because the motion of the reflectors imparts a measurable shift to the frequencies of the echoes.

Each of these modes has specific applications in clinical practice, with B-mode being the most versatile and widely used, especially in LUS for identifying key artifacts such as B-lines.

Ultrasound (US) offers several significant advantages that make it an invaluable imaging modality in modern healthcare. Its primary benefit lies in its non-invasive nature and exceptional safety profile. Unlike x-ray or CT, US uses mechanical waves, with no known risks of cumulative exposure, and not ionizing radiation. This enhanced safety makes it the preferred method for monitoring fetal health during pregnancy [Harrison, 2003].

Another key advantage of US technology is its versatility. Modern US systems allow for the acquisition of images with varying resolutions, depths, and angles, as well as the ability to visualize blood flow, all on the same device. This versatility, combined with real-time imaging capabilities, enables rapid data collection with minimal patient preparation time [Volpicelli, 2012].

Point of Care Ultrasound (POCUS), where physicians perform examinations at the bedside of unstable patients, is possible because of the high portability and modularity of US machines. Specifically for LUS, Lichtenstein notes, "Lung Ultrasound

allows fast, accurate, bedside examinations of most acute respiratory disorders" [Lichtenstein, 2014].

From an economic perspective, US is relatively inexpensive as compared to other advanced imaging techniques such as CT or MRI, allowing hospitals to save money without compromising patient care. This cost-effectiveness, combined with its wide availability in healthcare settings, means that expanding its capabilities would have a substantial impact on patient care.

Particularly in the context of COVID19, large benefits were realized in using US to scan the lungs. COVID19 had infected many people, making the speed at which patients could be evaluated even more important. POCUS permitted patients to be processed in place, thus reducing nosocomial infections through the elimination of the need to transport potentially infectious patients through the hospital. Surface disinfection protocols between exams were facilitated through the small surface area of US equipment. All of this made LUS a valuable screening tool for triaging patients when there were large numbers of cases and limited capacity in urgent care centers.

Apart from these fringe benefits, the analysis of LUS artifacts was very effective in the role of diagnosis and disease stratification of COVID19 patients [Ciurba, 2022]. LUS is even beneficial for evaluating asymptomatic patients with confirmed COVID19 [Lin, 2020]. As compared to chest x-ray all studies in a review paper showed LUS to have greater sensitivity with half having improved specificity [Chua, 2024]. LUS also compares favorably to CT, having a diagnostic agreement of 81% [Wang, 2021].

For these reasons POCUS rapidly became the preferred diagnostic and monitoring imaging tool for COVID-19 pneumonia. [Volpicelli, 2024].

While US offers numerous advantages, it is not without limitations. These can be broadly categorized into safety concerns, technical limitations, and operator dependencies, all of which must be handled appropriately.

Safety Concerns:

In typical US, the safety concerns are heating, radiation force, and cavitation. However, these can be easily managed by limiting the exposure time and intensity [Duck, 2008]. LUS specifically carries a potential risk of induced pulmonary capillary hemorrhage. Though this has only been observed to date in animals, it is suggested to further lower the mechanical index (MI) below the

standard safety setting of 1.9 MI [Moyano, 2022] to 0.4 MI [Miller, 2022] to minimize the risk.

Technical Limitations:

US has some technical constraints. While the axial resolution of most clinical systems is good (0.2-2 mm) it becomes worse when deep views that necessitate lowering the frequency are required [Azhari, 2020]. Also, US has a lower SNR than some other imaging modalities like x-ray, MRI and CT [Azhari, 2020]. Furthermore, diagnostic US cannot penetrate the entire body due to tissue attenuation and bright reflectors like bones. The penetration of LUS in particular is further limited by the lung surface when the lung is properly aerated.

Operator Dependencies:

US imaging quality depends a great deal on technicians being skilled and able to adapt. Yet even so an educational gap exists where medical students do not always have experience with ultrasound by the end of their undergraduate studies [Kameda, 2022]. The manual nature of US data collection introduces variability, and the diversity of clinical systems complicates cross-system comparisons [Volpicelli, 2012]. Additionally, scans of the same area can appear very different when using different probes, necessitating that probe type and parameters accompany US scans to aid in their interpretation [Volpicelli, 2012].

Despite these limitations, LUS represents a valuable tool for the monitoring of COVID-19 disease progression.

This thesis is structured as follows: First, a comprehensive background on lung ultrasound and B-lines is provided. Next, the existing literature on B-line formation theories is reviewed. Then the design of a novel model for the creation of vertical artifacts that highlights pleural involvement is detailed. Following this, the results showing that a membrane alone is sufficient for the production of vertical artifacts are discussed. Finally, the potential impact of these findings on LUS interpretation are addressed.

4. Background

4.1 Anatomy relevant to B-line formation.

Understanding the origin of B-line artifacts requires a comprehensive examination of the anatomical structures through which ultrasound waves propagate during LUS imaging. B-lines arise from the complex interactions between ultrasound waves and the structures of the chest wall and lung. Therefore, a knowledge of the anatomy is crucial for LUS interpretation and artifact analysis. The typical layers encountered, from superficial to deep, are:

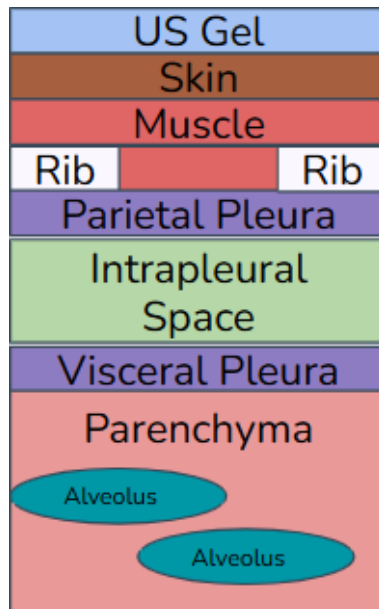


Figure 1: The anatomical layers encountered in lung ultrasound.

Coupling gel: An US technician will place a very thin layer of gel on the skin of the patient. This gel layer is often indistinguishable in the final image but serves the important role of eliminating air gaps between the transducer and skin that would disrupt optimal wave transmission to the underlying anatomy. It is not, though, part of the body and therefore not of interest in diagnosis.

Skin and intercostal muscles: These soft tissues appear as hypoechoic layers on the ultrasound image and do not contribute to an understanding of the state of the lung. The primary relevant effect of these tissues is to attenuate the signal.

Ribs: When ultrasonic waves meet dense materials such as ribs or other bones, bright reflections are created. Below these acoustic shadows are cast and everything below the reflector is obscured. LUS is performed in areas between the ribs where the lung can be seen which are termed "intercostal windows." This limits the area where a transducer can be placed to scan, so micro convex [Volpicelli, 2012] or phased array probes are often used since they provide a wide field of view fanning out from a small head surface area.

Pleural membrane: The pleurae are most hyperechoic when proximal to an aerated lung. Under ultrasonic inspection in healthy patients this membrane appears as a single, smooth and horizontal line due to its thinness. In reality, it is a double layered serous membrane that folds back on itself at the lung hilum. The total thickness of the pleura is approximately 200 µm, with each membrane being about 100 µm thick separated by 20 µm of intrapleural space [Gill, 2008]. When there is disease, the pleura can become irregular or thickened. B-lines, should they arise, begin from the pleura line [Volpicelli, 2012]. The pleura consists of three subparts:

Parietal pleura: This membrane covers the lung's surface and is in contact with the intercostal muscles.

Intrapleural space: Within this compartment is a minute amount of serous fluid. Throughout the breathing cycle this fluid is under 4 mmHg of negative pressure. This helps to keep the lungs inflated and sliding smoothly.

Visceral pleura: This membrane forms the actual surface of the lung. It is connected to the main tissue of the lung through the walls of the alveoli. Clefts where there are lobes. The membrane has many fine connections to the parenchyma, the walls of the alveoli, which are around 10 µm thick.

Lung parenchyma: This is the main tissue of the lung. It is elastic and displays hysteresis [Escolar, 2004]. Within it are the diminutive chambers of the alveoli where gas exchange occurs. In LUS, when there is proper aeration of the lungs, the parenchyma is not visible. However, when in a diseased state with flooded regions, namely consolidations, at the surface, B-lines can be seen. With increasing amounts of consolidations, the lung can experience "hepatization" where the lung resembles the liver in being echo-transparent [Marini, 2021].

Diaphragm: In scans of the lower lung the diaphragm can also be observed.

4.2 The importance of artifact analysis in LUS.

Artifact analysis is critical to the interpretation of lung ultrasound (LUS) images. In medical imaging the term ‘artifact’ refers to misrepresentations of tissue structures as a product of an imperfect image reconstruction method or other undesirable side effects of interactions that incoming signals have with the measuring system itself. While artifacts are often detrimental, in LUS they provide critical information.

The appearance and location of artifacts can be confusing and misleading without a good understanding of the factors leading to their genesis, because artifacts do not directly represent structural physiological reality in the same way the rest of the image does. Nevertheless, the presence in LUS of several classes of artifacts is not random as they do reflect true biological signals. Therefore, these artifacts can be used to signal the state of the lung with a proper theoretical model of the particular interactions of ultrasound waves and tissue interfaces that cause them. Knowing this allows artifacts to be analyzed so that more can be understood about the underlying physiology through their individual presentations.

B-lines are a prime example of the artifacts that play such a crucial role in LUS. A few of the other important artifacts which are commonly utilized in the evaluation of COVID19 by LUS are A-lines, lung sliding and pleural irregularities. Without analysis of B-lines and other key artifacts US would not be as useful a modality to investigate the lungs. More can be learned about the state of the lung by understanding the origin of B-lines.

Artifacts, such as B-lines, are important in LUS since not much structural information can be obtained by US of the lung itself when it is properly aerated. Structural information for the lung parenchyma is unavailable due to the high impedance at the lung surface. At the surface of the inflated lung, the peripheral region of soft tissue, comprising the layers of skin and muscle, has acoustic properties akin to those of water. The peripheral region then cedes to a region with a high air content. Consequently, there is an enormous resultant change in impedance, roughly that of water and air, which reflects 99.99% of the energy of impinging waves. Thus, views of all structures deeper than the pleural line are obstructed.

Consequently, there is a greater emphasis on information obtained by the analysis of artifacts to learn about the state of the lung. Although the ultrasonic waves cannot penetrate below the lung surface, LUS still provides valuable information about the state of the lung through the analysis of the artifacts in the section below.

4.3 Definition of important artifacts in LUS.

A-line: A-lines are horizontal hyperechoic artifacts that occur at multiples of the distance of the transducer to the pleurae. Their origin is well understood. They are the result of repeated echoes between the air-water interface at the pleural membrane and the transducer [Marini, 2021]. It is this reverberation that explains the periodic placement of these artifacts. Having strong A-lines is a marker of good aeration in the lungs and a positive sign for patient health. Among the elderly the A-line is often missing even absent of disease [Chiesa, 2014].

Lung sliding: This artifact is seen as a horizontal motion at the pleural line when viewed in B-mode. A similar artifact can also be seen in M-mode where it is known as the seashore sign [Łyżniak, 2023]. Lung sliding is also a positive sign of normal function.

Pleural Irregularities: Pleural irregularities lie somewhere between a sign and an artifact. They are loosely defined as discontinuities or thickening of the pleural line. Notably, across the literature, there is little quantitative standardization of this definition [Demi, 2022b]. This is in part due to its highly varied presentation. According to Marchetti pleural thickening can be echogenic or echo-poor, diffuse or focal [Marchetti, 2018]. A pleural line with an irregular jagged appearance in LUS is the result of subpleural consolidations [Soldati, 2017]. At least some differences in the pleura do reflect structural deviation of shape. As is common in COVID19 [Adams, 2020], a thickened pleura seen in LUS can often also be seen on CT [Adams, 2020] [Saha, 2021]. It is likely that pleural irregularities are more prevalent but are understudied in favor of the parenchyma [Saha, 2021]. In COVID19 discontinuous Pleural Irregularity is often observed as well. In the future pleural thickening as opposed to irregularities may become recognized as two separate clinical signs.

Light Beam: This artifact is not mentioned by many groups. It was defined by Volpicelli as a broad lucent band that appears and disappears with lung sliding. It is seen in the same patients with covid19 pneumonia that show Ground Glass Opacities (GGOs) in CT [Volpicelli, 2020]. This reported artifact may in fact be grouped B-lines that are moving together and not its own artifact.

White lung: An ultrasound finding characterized by a uniformly hyperechoic lung field with a superimposed coalescence of multiple B-lines, which obscure the normal horizontal reverberation patterns typically seen in healthy lung tissue [Soldati, 2009].

4.4 Definition and characteristics of B-lines.

One of the main artifacts observed in covid patients are B-lines [Demi, 2022b]. A definition of B-lines laid out by the first international consensus conference on LUS was “discrete laser-like vertical hyperechoic reverberation artifacts that arise from the pleural line (previously described as ‘comet tails’), extend to the bottom of the screen without fading, and move synchronously with lung sliding” [Volpicelli, 2012]. The second conference pointed out the weakness of the definition, namely the subjectiveness of these characteristics and how it ignores the effects of key imaging factors on their appearance [Demi, 2022b]. However, while they encourage the development of a more quantitative definition, they did not suggest an updated definition.

An earlier definition by Lichtenstein additionally listed the erasing of A-lines as a characteristic of B-lines [Lichtenstein, 2008]. This earlier definition has not yet been entirely supplanted by that of the second international consensus conference [Volpicelli, 2012] in the literature, still appearing in some papers [Łyżniak, 2023] [Lichtenstein, 2014]. B-lines are often concurrent with a thickened and irregular pleura. In the elderly A-lines are less common and it has been suggested that this is due to them having irregular pleurae. B-lines are correlated with earlier stages of extravascular lung water. As areas of the lung increase their water content B-lines will get grouped together, or ‘confluent’, and near full consolidation they disappear again. The finding of B-lines by LUS is highly correlated with the finding of GGOs on CT.

During the progression of COVID19 B-lines appear early on [Volpicelli, 2020]. At first there are only a few individual B-lines. As the disease gets more severe more and more B-lines appear. The B-lines can become very numerous and closely spaced. Confluent B-lines are a sign of moderate to severe disease. With further deterioration the lung might develop large consolidations where the B-lines are no longer seen. Alternatively, the lung may get to the White Lung state and be nearly fully hyperechoic.

4.5 Disambiguation of B-line terminology

The literature is not consistent on the nomenclature for B-line artifacts. The early papers in this fast-evolving field had to create their own terms to describe the phenomenon they were observing. Among the early names in circulation for B-lines were “ring-down artifacts” [Avruch, 1985], “comet-tail” [Lichtenstein, 1997] and “lung comets” [Jambrik, 2004] “B3–B7 lines” [Blanco, 2016], “I/Z lines”, “lung rockets”, “ULCs”, and “light beam” [Smargiassi, 2022]. In these early works these terms were used interchangeably causing confusion that made it difficult to coordinate and converse on the topic. At the first consensus conference on the LUS leading members of the field settled on the name B-lines and standardized the definition [Volpicelli, 2012]. Since this has mostly been adhered to although there are exceptions.

Several other LUS signs are described in the literature which are similar to B-lines either in appearance or name. Some of these may simply use different terminology to describe the same phenomenon. For example, “lung rockets” was used to discuss multiple confluent B-lines until it was later supplanted by the term B-pattern in the first lung ultrasound consensus conference [Volpicelli, 2012]. Łyżniak lists an impressive host of artifacts from A-lines to Z-lines [Łyżniak, 2023]. There are other artifacts that share an appearance with B-lines but are not the same since definition B-lines occur in the lungs; they can theoretically even share a mechanism of formation. An example of this would be the R-lines arising from the pericardium or E-lines from subcutaneous air bubbles [Łyżniak, 2023].

Some groups have attempted to improve the clarity and specificity of the terminology used around LUS vertical artifacts by drawing distinctions between different sets of terms. One group tried to draw a distinction between B-lines and CTAs stating that when the artifact arises from a smooth pleural line it is the former and from an irregular one the latter [Mathis, 2021]. Another group [Lee, 2018], without providing new evidence, suggests that artifacts should be named after their source mechanism of formation; either Ring Down artifact if from a bubble tetrahedron or Comet Tail artifact if from a large impedance mismatch. A final group [Buda, 2021] went in the opposite direction blurring the distinction between Z-lines, short vertical artifacts that are not clinically relevant, and the long pathologic B-lines. They described the interconversion of B and Z lines based on frequency of insonation. It is not clear how much support these positions have.

A great deal of imprecision still exists in the literature discussing B-lines with many terms coined for what are not likely truly distinct phenomena. Comet-tail artifacts are still the accepted name for the vertical reverberation artifacts like those from foreign

bodies such as glass and metal or calcifications [Morgan, 1991] [Tchelepi, 2009] [Wu, 2018]. See figures 2 and 3 for examples from the lab of the vertical artifacts that glass and metal can produce in a water bath. However, in the interest of clarity, this work will adopt the term vertical artifact [Smargiassi, 2022] as a catch-all term for artifacts short or long which resemble B-lines and when discussing synthetic artifacts. The term B-lines is used to discuss only the ‘long’ laser-like artifacts in the lung while Z-line is used for short lung artifacts.

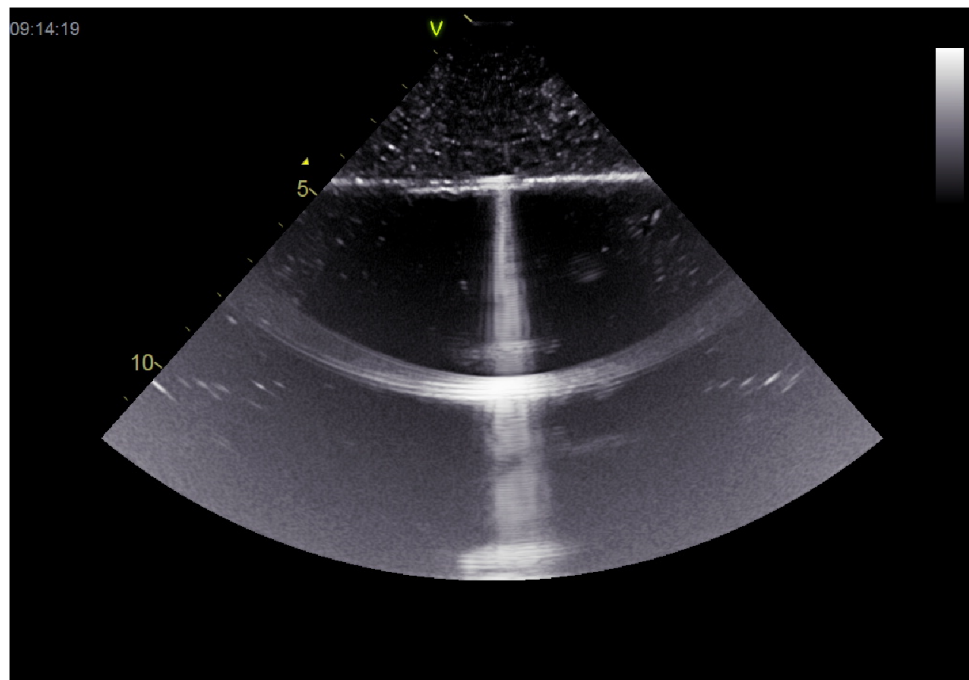


Figure 2: An in vitro metal “foreign-body” artifact.

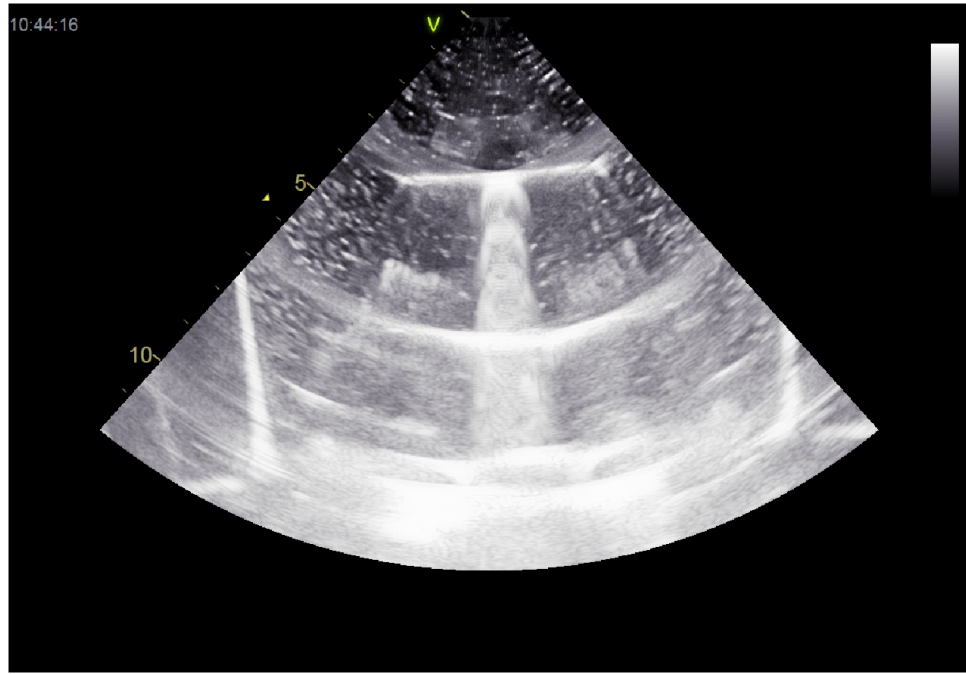


Figure 3: An in vitro glass foreign-body artifact with modulation.

4.6 Clinical significance of B-lines in various conditions.

In the evaluation of COVID19 severity, B-lines are analyzed in the clinic in a semi-quantitative manner. Utilizing a 12-zone scan protocol, patients get an overall score depending on how many B-lines are observed in their exams [Soldati, 2020]. This method of lung scoring is only semi-quantitative because of the large number of operator dependent parameters that can change the appearance of the B-lines and the lack of a single cross-platform protocol for their settings [Demi, 2020a]. Despite this, LUS findings from 12-zone lung scoring protocols correlate to CT findings and can be useful for monitoring changes in COVID19 pneumonia [Haurylenka, 2021]. For COVID19 a higher number of B-lines correlates with worse patient disease states [Lopes, 2020].

Throughout the course of the COVID19 pandemic LUS 12-zone Lung score protocol was used mostly as a screening tool because of its high sensitivity but lower specificity. Since the presence of B-lines is not pathognomonic, without additional information it cannot be definitively stated which of a range of potential conditions a patient may have [Safai, 2024]. So, other information such as patient history is still

necessary for a diagnosis and the gold standard for diagnosis remains a molecular RT-PCR test.

Indeed, the range of diseases for which B-lines can be a clinical marker is wide. These include various conditions where there is extravascular lung water [Jambrik, 2004] such as cardiogenic pulmonary edema, noncardiogenic pulmonary edema, interstitial syndrome, pneumonia, ARDS, alveolitis and also some where there is not additional extravascular lung water like pulmonary fibrosis [Demi, 2022a] [Gargani, 2009] [Manolescu, 2018].

It is also possible to observe a few individual B-lines in the base of the lungs of healthy people [Lichtenstein, 1997] [Bhoil, 2021] [Sperandeo, 2012]. It is also common to see B-lines among the elderly without an “anterior infraclavicular to posterobasal” gradient [Chiesa, 2014]. For this reason, having fewer than 3 B-lines in an ‘intercostal window’ is usually not considered significant. The threshold for clinical relevance is usually three lines in a single intercostal window [Bhoil, 2021].

Analyzing B-lines is useful in a trauma setting too [Stone, 2009]. The presence of B-lines can exclude a pneumothorax at a given point as they indicate contact of the visceral and parietal pleura [Volpicelli, 2012] For the diagnosis of a pneumothorax as opposed to chest x-ray the specificity of POCUs is similarly high and nearly twice as sensitive [Alrajab, 2013].

Similarly, according to Lichtenstein (1998) Chronic Obstructive Pulmonary Disease (COPD) and edema can be differentiated by the presence of B-lines. COPD looks normal on LUS as opposed to edema which presents B-lines since COPD affects the inner lung and edema is diffuse.

The ultrasound finding of confluent B-lines in COVID19 is equivalent to the finding of GGOs on CT [Tung-Chen, 2020].

The distinction between diffuse and focal patterns of distribution is also valuable diagnostically, helping clinicians differentiate between various lung pathologies beyond COVID-19. This is already used a bit [Copetti, 2008]. Diffuse patterns are observed in conditions such as Acute Respiratory Distress Syndrome (ARDS), Cardiogenic Pulmonary Edema (CPE) [Copetti, 2008], Diffuse Alveolar Hemorrhage (DAH), and other conditions like idiopathic pulmonary fibrosis. Focal B-line patterns, on the other hand, are associated with conditions including, interstitial pneumonia [Volpicelli, 2009] atelectasis, pulmonary contusion [Soldati, 2006], pulmonary infarction, pleural disease, and neoplasia.

4.7 Expanding the suite of features.

B-lines contain more information than solely their frequency of occurrence. Beyond a simple count of the B-lines, as employed in the lung scoring protocol, several other B-line characteristics merit consideration.

Spatial distribution is one such feature. B-lines can be categorized as either diffuse or focal in their pattern, (as mentioned in the previous section). Additionally, the anatomical location of B-lines is significant; those appearing towards the lung base are generally considered less clinically relevant.

Other B-line features, though less extensively studied, show promise in refining diagnostic capabilities:

- Fundamental frequency: Demi et al. (2017) suggest that B-lines have a fundamental frequency that may indicate the size of disease affected lung areas.
- Frequency range: Buda et al. (2021) propose that the range of frequencies at which B-lines are visible could offer similar information without requiring spectrographic analysis.
- Modulation: The patterned variation in B-line intensity along the axial direction, as described by Avruch et al. (1985), may provide additional diagnostic insights.
- Beam width: The width of B-line artifacts could potentially correlate with the extent of lung tissue alterations.
- Axial Extension: The length of a B-line may be relevant in determining lung health.

Wang et al. (2022) explored quantitative features of B-lines for computer-aided diagnosis, including:

- a) Accumulated Width of B-Lines
- b) Attenuation Coefficient of B-Lines
- c) Accumulated Intensity of B-Lines

Interestingly, Arntfield et al. (2021) demonstrated that a deep learning model trained on B-line images could outperform human experts in distinguishing between lung pathologies. While the specific features utilized by the model remain unclear, this study suggests the presence of subtle characteristics not readily apparent to the human eye still to be uncovered.

This expanding suite of B-line features holds promise for enhancing the diagnostic and prognostic capabilities of lung ultrasound. Further research such as this work is needed to fully elucidate the physiological meaning of these features and their clinical significance. Then these characteristics will be able to be integrated into standardized assessment protocols.

4.8 Challenges in analyzing B-lines.

Unfortunately, despite the potential wealth of information contained in B-lines, clinicians face several challenges to fully utilizing all the information of ultrasound artifacts for diagnostic purposes. These challenges stem from technical limitations, theoretical gaps, and practical difficulties in data collection and analysis.

Technical Limitations of Clinical Ultrasound Machines

Most clinical ultrasound machines are not optimized for advanced spectrographic B-line analysis. The majority of commercially available US machines do not allow recording of raw radiofrequency (RF) data, which is necessary for advanced signal processing [Demi, 2014]. Instead, these machines typically store only processed images with reduced spatial frequencies, often further compressed to save storage space. This impedes the adoption of spectrographic approaches and other advanced analysis techniques.

Theoretical Gaps in B-line Formation Models

The lack of a widely accepted theoretical model for B-line formation presents another significant challenge [Kameda, 2021]. This theoretical uncertainty makes it difficult for physicians to interpret and trust new analyses based on additional B-line features, as the clinical significance and physiological meaning of these features remain unclear.

Saturation and information loss

A-line and B-line artifacts are often strong enough that they saturate the detection settings for returning pressure waves. This leads to the loss of information making it difficult to compare magnitudes of B-lines on even the same scan.

Standardization and Reproducibility Issues

The lack of standardized protocols for B-line acquisition and analysis poses additional challenges. Different ultrasound machines, settings, and operator techniques can all influence the appearance and characteristics of B-lines, making it difficult to compare results across studies or clinical settings.

4.9 Physics of Lamb Waves.

Lamb waves are a special type of transverse surface wave that occur in thin plate or cylinder solids. Lamb waves are noteworthy for being good at traveling long distances with low energy losses.

The study of Lamb waves is most common in Non-Destructive Examination (NDE) for industrial purposes. They play a crucial role in ultrasonic testing to ensure part integrity and verify the absence of delaminations in composite materials. Beyond industry, Lamb waves have also made inroads into medical applications, particularly in the analysis of bones, cornea, and thin-walled structures such as the aorta.

As opposed to the similar Rayleigh waves, Lamb waves only propagate in thin plates of materials when their thickness is on the order of the wavelength of the compressional speed of sound in the material.

There are two main families of lamb wave vibrational modes, namely, symmetric and antisymmetric. The symmetric modes are characterized by compressive, in-plane movements, while antisymmetric modes exhibit flexural, out-of-plane movements. Antisymmetric modes are of particular interest in fluid-solid interactions, as they have the potential to interact with fluids in contact with the material surface, potentially leading to energy transfer from the plate to the fluid.

The experiments described in this work suggest a connection between Lamb waves and the formation of B-line artifacts in lung ultrasound. The thin membrane lining the lung appears to act as a conduit for energy transfer, with fluid loading on one side and a free air-coupled side on the other. This observation has significant implications for the interpretation of lung ultrasound artifacts.

Given that physicians rely on B-Line artifacts to make critical patient-care decisions, there is a need to better understand their underlying mechanisms. Knowing

their cause would enable a more methodical analysis of these artifacts. Moreover, a robust theoretical model explaining the physiological meaning of B-lines would instill greater confidence in physicians to utilize them.

5. Literature-Review

The physiological mechanism explaining B-line artifact formation in lung ultrasound has been a subject of research and debate over the past four decades. This literature review aims to provide a comprehensive overview of the current state of knowledge regarding B-line generation. The review will begin by examining the three principle theories that have emerged to explain this phenomenon: the resonance theory proposed by Avruch in 1985, the reverberation theory put forward by Lichtenstein in 1997, and the acoustic trap theory introduced by Soldati et al. in 2009. Each of these theories offers a unique perspective on the underlying mechanisms of B-line formation, reflecting the evolution of understanding over time. Following this theoretical discussion, the review will explore the various experimental models and methods that researchers have employed to recreate and study B-lines in controlled settings. These models include both simple physical analogues and digital simulations. By critically examining both the theoretical frameworks and the practical approaches to B-line research, this section will contextualize the current study within the broader field of lung ultrasound research and highlight the gaps in knowledge that the present work seeks to address.

5.1 Theories of B-line Formation

Resonance Theory (Avruch)

In 1985, only a few years after the first reports of vertical artifacts in ultrasound, Avruch and Cooperburg proposed the first theory attempting to explain the cause of the vertical artifacts in lung ultrasound that would come to be known as B-lines. Their paper "*The Ring-Down Artifact*" laid the foundation for the resonance theory of B-line formation.

The authors conducted experiments using a model composed of bubbles in soapy water and gelatin. In each medium, the bubbles were arranged in a specific geometry so that they created a tetrahedron, with three bubbles forming the top layer

and one nestled beneath. Refer to Figure 4 for a visualization of the arrangement of the bubbles.

The authors successfully generated vertical artifacts resembling B-lines using their bubble model. They posited that the “bugle-shaped” fluid volume trapped within the tetrahedron was resonating when struck by the ultrasound and this caused it to send out a continuous signal back to the transducer. Their model was not difficult to replicate and the artifacts it forms can be seen in Figure 5 where vertical artifacts emanate from a tetrahedron of soap bubbles held beneath an inverted plastic cup in a water bath.

Avruch and Cooperberg extrapolated their findings to lung pathology, suggesting that as fluid accumulates in the lung parenchyma during disease states, similar resonating structures could form, leading to the production of B-lines.

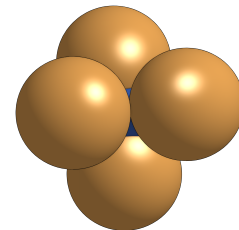


Figure 4: 3D model of Avruch's bubble tetrahedron.



Figure 5: Experimental replication of Avruch's "Ring Down Artifact."

Reverberation Theory (Lichtenstein)

Over a decade later, in 1997, Lichtenstein and colleagues published their paper titled "*The comet-tail artifact: An ultrasound sign of alveolar-interstitial syndrome*". There they proposed an alternative explanation for the formation of vertical artifacts in lung ultrasound. Unlike Avruch and Cooperberg's model-based experiments, Lichtenstein's work was grounded in clinical observations of 250 consecutive patients in a medical intensive care unit. Lung ultrasound findings were compared with chest radiographs and CT scans, focusing on the antero-lateral chest wall. They called the artifacts observed "comet-tail artifacts" (now commonly known as B-lines). The authors found a strong correlation between what they called comet-tail artifacts and alveolar-interstitial syndrome.

Lichtenstein and colleagues proposed that B-line formation was the result of reverberation, suggesting that these artifacts are formed by multiple reflections of the ultrasound beam in thickened interlobular septa, where there are rapid changes in acoustic impedance. This is why the name chosen for the artifact was the same as that given by Ziskin to the vertical artifacts caused by the shotgun pellets in the liver. Both sets of authors identified the phenomenon with reverberation.

This work was also important because it encouraged the early adoption of clinical LUS. The authors discussed several of the key LUS signs still in use today, proved their use in diagnosis and demonstrated how these findings were comparable to CT. Furthermore, they showed that the location of B-lines could signal a differential diagnosis.

Lichtenstein and colleagues' theory differed from Avruch and Cooperberg's theory in several key aspects. It focused on reverberation rather than resonance as the primary physical phenomenon, emphasized interlobular septa rather than air-fluid interfaces in alveoli, and demonstrated direct correlation with pathological states, suggesting potential for widespread clinical use. This work laid the foundation for much of the subsequent research and clinical use of B-lines in diagnosing and monitoring lung pathologies.

Acoustic Trap Theory (Soldati)

The next important work "*Sonographic Interstitial Syndrome: the Sound of Lung Water*" was published by Soldati and colleagues in 2009. This work presented a novel

theory for the formation of B-lines, building on previous research but offering a more comprehensive physical explanation for the phenomenon.

Soldati et al. conducted both clinical observations and experimental models to investigate the nature of B-lines. Their study involved patients with various lung pathologies, including cardiogenic pulmonary edema and ARDS, as well as in vitro experiments using gelatin phantoms with air inclusions.

The authors proposed that B-lines are formed due to acoustic trapping within fluid-filled structures in the lung, rather than simple point-source reverberation or resonance. They suggested that when portions of the lung surface become less aerated, ultrasonic waves can penetrate through these fluid-filled channels into the lung parenchyma. Here the interfaces between fluid and air in unmodified lung tissue trap the waves. These "acoustic traps" would preferentially capture frequencies that match the size of the trap's internal reverberations. As the trapped waves slowly leak out and return to the transducer a characteristic vertical artifact would be formed.

Soldati et al. (2009) also presented important arguments for the rebuttal of the previous two theories. Pointing to their experiment, in which a single layer of bubbles at the air-water interface of a water bath that was scanned from below produced vertical artifacts, the authors argue that the specific tetrahedral geometry described by Avruch was not necessary to create vertical artifacts. However, this argument may be considered insufficient, as a volume of fluid would still be trapped at the interface and between the interface and bubbles, potentially allowing for the formation of artifacts. This is their weakest point, but their only one based on their own work as described in this paper.

Soldati et al. 2009 went on to argue that the mechanical properties of the liquid or tissue volume trapped between the bubbles make it mathematically impossible "*to have vibrational resonance in the high-frequency bandwidth of ultrasonic pulses*" [Soldati, 2009]. Their final argument against Avruch is that the central frequency of the artifacts noted by Avruch was more likely to be the result of reverberation than resonance since they were lacking the harmonic response signal which would be expected of a nonlinear resonator. The authors also discounted the theory of Lichtenstein because the interlobular septa could not explain all the diseases in which B-lines are seen and the B-lines distributions do not actually line up with the anatomy of interlobular spacing as Lichtenstein had believed.

This theory of B-line formation has become the most popular [Demi, 2022b] with many groups building off of it [Soldati, 2011] [Soldati, 2016] [Leote, 2023] [Demi, 2018] [Demi, 2021] [Buda, 2021].

An important corollary of this theory is that the size of acoustic traps would determine their native frequency, with an inverse relationship between their physical dimensions and said native frequency [Demi, 2020b].

5.2 Models for B-line Generation

In order to study the formation of B-lines, special “phantoms”, or models, are required. Lung tissue, as opposed to other organs, contains a lot of air. The lungs are complex organs with many fine features, like the thin-walled alveoli, that begin to degrade soon after death. Efforts to remove this organ can easily damage the fine structures we wish to examine, and preservation techniques disrupt the distributions of fluid in them. Therefore, most works with the aim of explaining the origins of B-line focus on producing models of the lungs and not working with the tissue itself. There has been at least one paper published that used an excised lung and performed histological studies [Soldati, 2012]. However, that work had no benefit towards isolating a formation mechanism of B-lines or for establishing a method for differential diagnosis based on B-lines. For these reasons as well as reproducibility and durability using model systems is preferred to real tissues for the study of B-lines.

Physical Models

Sponges

Many of the physical models were made to simply mimic the wet spongy character of diseased parenchymal lung tissue with many small, interconnected chambers. While naive, this approach is fruitful in that it creates vertical artifacts. There have been studies using both sponges [Bluthgen 2017] [Leote, 2023] and dressing materials [Park, 2017]. These models are usually very low cost and could be useful for education of technicians or testing various ultrasound parameters' effect on artifact presentation, but they do not isolate any mechanism of artifact generation.

Bubbles

Several models were made around the concept of using bubbles to represent the aerated spaces of the lung. One of the advantages of this was that experimenters were able to have a more sophisticated control of some of the parameters in the model like the geometry of bubble arrangement and the size of the bubbles used. Different studies employed different arrangements of bubbles from the bubble tetrahedron to single, from bubble chains to single or multiple stacked sheets of bubbles and even monodisperse bubble clouds [Demi, 2017]. Potential points where this model differs from the true lung are the dimension of the simulated versus actual alveolar walls and the fact that the bubbles are not interconnected.

Air rods

Under this approach models were constructed by pushing rods through drilled holes in the sides of a box. Then a gel mixture was poured in. Once the gel had cooled and settled the rods were removed leaving behind aerated spaces. This method allows for much more control over where the aerated spaces appear in the model and allows the effect of their geometric arrangement to be investigated. One such investigation was carried out by Demi (2021).

Gel shapes

In other studies researchers thought a little more outside the box. In these studies, differently shaped gel objects like hemispheres [Kameda, 2022] or agar “cusps” [Demi, 2021] were placed outside the main acoustic conducting volume so that they were surrounded by air save where they contacted the main body of the model. These are good models for micro consolidations in the subpleural space.

Another paper also tangentially reported an artifact arising from the edge of a gel disk under membrane [Demi, 2023].

Falling water droplet

One of the more unique models was made by Demi et al. in 2023. This model consisted of a container of water with a hole in the bottom. The researchers used ultrasound to watch a drop of water drip down from the container. Soon before each drop fell a vertical artifact could be briefly seen. The motion within the model reduces the similarity to the physiology and potentially interferes with the scan. Also, the brevity of its appearance reduces confidence that this is analogous to the stable reproducible B-lines seen in LUS.

Digital Models

Two main works with the same primary author were identified that attempted digital simulations of the formation of B-line artifacts. These works differed both in their approach and in the software used.

Kwave

In 2022, Da Silva et al. made a digital model in k-wave. The model was based around the ideas of acoustic traps and is most analogous to the air rod experiments done by demi. The digital phantom was constructed using groups of circles with specific acoustic properties to form the different regions. Circles with properties of muscle were stacked above smaller circles with properties closer to air and two circles representing water were superimposed on the circle of the air region. The water circles were horizontally centered just touching the interface and the distance between them was varied for different conditions. A hazy wide artifact was able to be produced, but it was not laser-like and there was no change to the A-line. This model takes a long time to run because k-wave does not handle very high impedance changes well even after the air was simulated using non-physically representative higher values. It is also not possible to model resonance with the k-wave code, so what was observed was only the product of reverberative reflections. [k-wave]

COMSOL

In a different paper Da silva 2022 used the COMSOL program instead [COMSOL]. COMSOL is a more sophisticated multiphysics simulator. Here a Lung Disease Zone (LDZ) was simulated projecting into the aerated section of the lung. The region above the lung surface was modeled with simple tissue parameters and below the lung surface with those of air. The acoustic property values within the LDZ had a large degree of heterogeneity and were centered around three quarters of the properties for muscle. This digital phantom successfully made b-lines but only with high tissue heterogeneity. There was also no erasure of A lines in the simulated images. This model was similar to the gel cusps of hemispheres physical models.

6. Methodology

In this work, as in previous literature, experimental phantom models were used to investigate the origins of the key LUS B-line artifact. Rather than involving patients, these *in vitro* models were designed to recreate the artifact under controlled conditions, allowing for optimal isolation of the underlying physical mechanisms. The present work employed three principal models. The first of these shared several features with setups previously fabricated by other research groups and served to inspire the development of more novel subsequent models. These models aimed to elucidate the contribution of the pleural membrane to the formation of LUS vertical artifacts.

6.1 Wrapped Sponge

Model Description

The Wrapped Sponge model was designed to simulate the complex structure of lung parenchyma and its interaction with ultrasound waves. A natural sea sponge partially saturated with water served to mimic the lung parenchyma. It was enclosed within a thin plastic wrap standing in for the pleural membrane. This setup allowed for controlled manipulation of the fluid content of the sponge while maintaining a consistent external boundary.

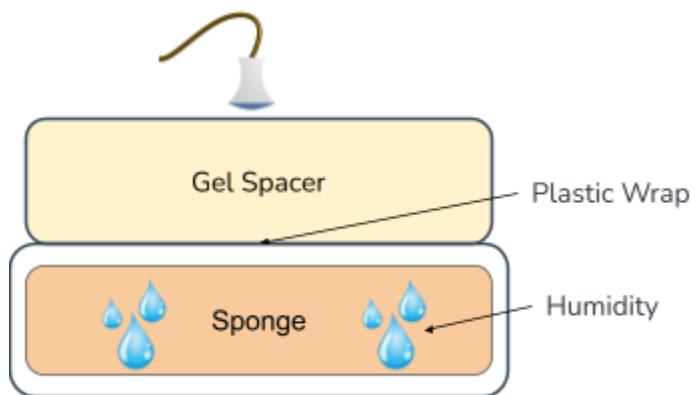


Figure 6: Wrapped Sponge model construction.

Model Construction

Components:

- Natural sea sponge (pore size range: 0.2-0.5 mm)
- Distilled water (for controlled saturation)
- Food-grade plastic wrap (PVC; thickness: ~0.2 mm)
- Agar gel spacer (3 cm thickness, 9 cm diameter)
- Ultrasound coupling gel

Procedure:

- A. The sponge was weighed in its fully dry state and its fully saturated state, which were found by squeezing the sponge underwater and removing it without squeezing, waiting for it to stop dripping (precision: ± 0.1 g).
- B. The sponge was then saturated to the desired level using a calculated volume of distilled water, based on the following equation:

$$(Eq. 3) \quad SF (\%) = [(W_w - W_d) / (W_f - W_d)] \times 100$$

Where: SF = Saturation fraction, W_w = Wetted weight, W_d = Dry weight and W_f = Fully saturated weight

- C. The partially saturated sponge was carefully wrapped in plastic film, ensuring no air pockets were trapped between the sponge and the wrap at the top surface.
- D. An agar gel spacer was placed on top of the wrapped sponge to provide a consistent acoustic pathway at a depth near that of the lung surface in typical patients.
- E. Ultrasound coupling gel was applied between the transducer and agar gel spacer, and between the agar gel spacer and the plastic wrap to ensure optimal acoustic transmission.
- F. The assembled model was scanned from above, with the ultrasound focus depth set at the interface between the agar gel and the plastic wrap (simulated pleural line).

Agar Gel Spacer Preparation:

- A. 200 ml of distilled water was brought to a boil in a beaker.
- B. Heat was reduced, and 12 g of gelatin powder was added under continuous magnetic stirring until fully dissolved.
- C. 6 g of agar powder was then added, and the mixture was stirred for an additional 30 minutes at medium heat.

- D. Any bubbles or foam were carefully removed to prevent superfluous sources of acoustic artifacts.
- E. The mixture was poured into molds and allowed to set, resulting in spacers of 3 cm thickness and 9 cm diameter.

Imaging Parameters:

Imaging was conducted using a GE Alton S70 ultrasound research system (GE Healthcare, Chicago, IL, USA) equipped with a 12S phased-array sector probe. These settings were chosen to optimize visualization of potential B-line artifacts while maintaining clinically relevant imaging conditions. The following imaging parameters were used:

- Frequency: 4.5 MHz
- MI of 0.7
- Depth: 6 cm
- Gain: 0 dB
- Dynamic Range: 65 dB
- Focus: Set at the simulated pleural line interface

Experiment: Change the water fraction of the sponge.

In this series of experiments sponges with different water loading percentages were compared. The different quantities of water simulate the lung tissue with increasing levels of extravascular exudate observed in many of the diseases where B-lines can be seen.

The sponges were loaded with water then shaken to slowly and evenly remove water down to the desired level. The sponges were ready to be wrapped when their saturation level was within 1 percent of the target saturation percentage.

After scans the sponges were weighted again to ensure that the saturation percentage had not changed during the experiment. If the weight had gone up the data was discounted. Similarly, if the weight went down by more than 2 percent the data was discounted as well. Discounted experiments were repeated.

Three different sponges were used and three images were taken of each at every condition. All other factors were kept equal.

The saturation levels used were 0, 10, 25, 35, 60 %.

6.2 Membrane Vice

Model Description

This model was designed to isolate the pleural membrane. The entirety of the real geometry peripheral to the lung surface was modeled as simple water and below the lung surface as air. Meanwhile, the porous nature of the parenchyma was ignored. The reduction in complexity of this model, displayed in Figure 7, from the biological lung is dramatic and allows for the isolation of the area of study.

To limit the motion of the membrane and maintain in it a specific fold conformation, a vice was built to hold the membrane. The vice was modeled in CAD and then produced in the faculty workshop out of Perspex/PMMA. The inner ring, colored green in the model displayed in Figure 8, is solid while the split outer ring can be fastened over the edges of the membrane and the legs reattached.

The decision was made to manufacture the vice without using metal parts so that additional vertical artifacts that could interfere in the experiment would not be created. For this reason, plastic screws were used to hold the vice closed. When placed in a water bath the fully plastic vice holds folds in the membrane surface and traps air below it, recreating the air-water interface at the surface of the lungs.

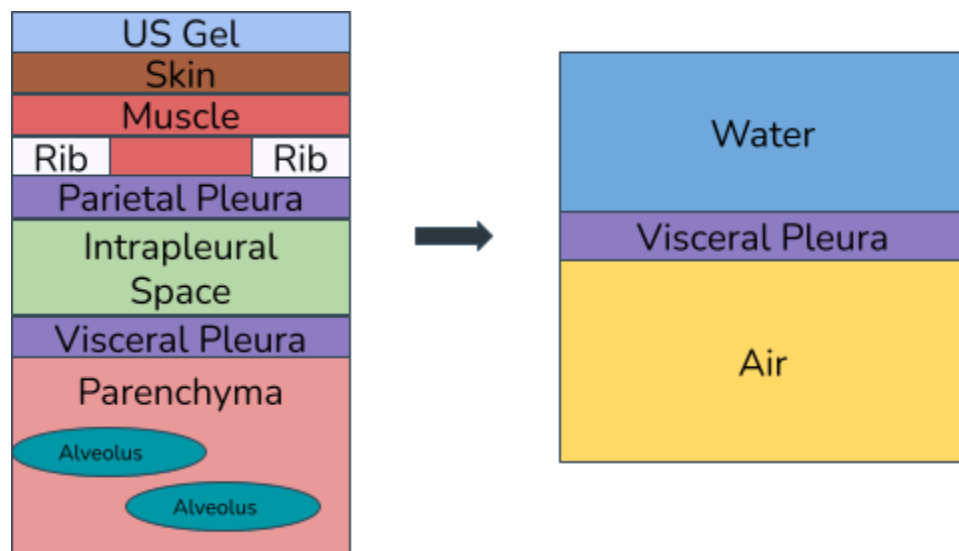


Figure 7: Conceptual simplification of the Membrane Vice model.

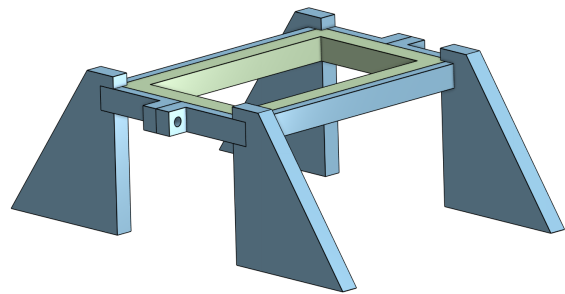


Figure 8: 3D CAD design of the Membrane Vice.



Figure 9: Membrane Vice experimental setup.

Model Construction

Components:

- Plastic Vice
- Plastic wrap
- Sausage Casing
- Vinyl rubber gloves
- Water bath

Procedure:

- A. The water in the water bath is degassed to remove excess gas that obscures the view under ultrasound. This is achieved by pumping water through small pores, which lowers its pressure. The water then enters a demixing chamber where

microbubbles coalesce to form larger bubbles. These larger bubbles float to the top of the bath and are eliminated.

- B. The vice is opened.
- C. A fold is made as desired in the membrane, and it is placed in the vice.
- D. The vice is then closed to secure the membrane in place.
- E. Extra metal weights are secured to the ends of the legs so the vice would not float. (These pieces of metal are far enough to the side that they do not appear in the field of view and thus do not interfere with the experiment).
- F. The whole vice is lowered slowly and evenly into the water bath so that there is a bubble of air trapped below the membrane.
- G. The model can now be imaged from above.

Imaging Parameters:

Imaging was conducted using a GE Alton S70 ultrasound research system (GE Healthcare, Chicago, IL, USA) equipped with a 12S phased-array sector probe. These settings were chosen to optimize visualization of potential B-line artifacts while maintaining clinically relevant imaging conditions. The following imaging parameters were used:

- Frequency: 4.5 MHz
- MI of 0.7
- Depth: 10 cm
- Gain: -1dB
- Dynamic Range: 65 dB
- Focus: Set at the simulated pleural line interface

Experiment: Change the shape of the fold in the membrane.

This experiment changed the shape of the investigated fold. The types of folds tried were concave convex or a simple folded over.

The Simple Fold over was done with 5 mm between the fold edges.

The Concave could be made either by pinching a 5mm length of the membrane on either side and then locking it in the membrane or pinching together material of 2 cm together on one side of the membrane. The first option was used, and this manual method was employed for both Concave and Convex folds.

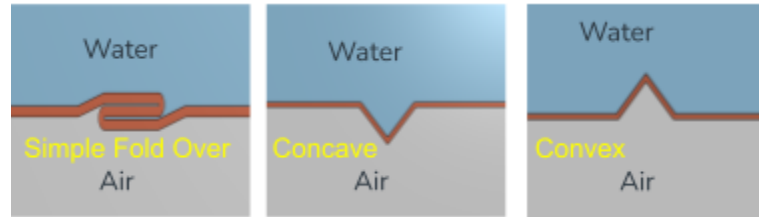


Figure 10: Membrane fold geometries in the Membrane Vice.

Experiment: Change the Material of the membrane.

In these experiments the material used for the membrane was varied. This simulates the visceral pleura during disease conditions where its material properties undergo change, i.e. pleural fibrosis and calcification. This experiment aims to provide insight into the effects of pleural material properties on B-lines. Three materials used as the membrane were compared: plastic wrap, sausage casing and vinyl rubber. Since sausage casing is gelatin based it is likely to have material properties that best match the pleura. The membranes were all given a convex fold.

Experiment: Using a bag as the membrane. Dry inside.

Since all materials used in the vice model; water, air, the membrane and the vice itself, were transparent it was difficult to know if the membrane lowered into the water bath stayed fully dry underneath. If water drops were on the underside, it might be that the water drops are the source of the vertical artifacts. Therefore, this experiment was conducted to fully eliminate the possibility that there was splashed water on the backside of the membrane in the vice.

To do this, instead of a sheet, a plastic bag was used. One side of the bag was secured in the vice with a fold then it was filled with dry air, not breath, and tied closed. This ensured that there would be no water droplets on the membrane's underside.

6.3 Pith Pits

Model Description

In this experiment a new material was used in B-line formation experiments. This model was prepared by isolating the pith from the rind of a large citrus fruit, pomelo. The advantage of using this material is that its surface can be modified without the whole model filling up with water. It can also stay submerged for a long time without losing its air. This can be easily verified by seeing that when submerged and pressed air bubbles leak out of the pith.

Only the spongy white air-containing tissue of the peel is used. The top layer of the peel containing the flavonoid oil glands must be removed because these produce their own small artifacts, but it is necessary to isolate the mechanism.

A hole of chosen dimensions is made in the top of the peel to represent areas of lung disease near the lung surface but importantly there is no pleural membrane involved.

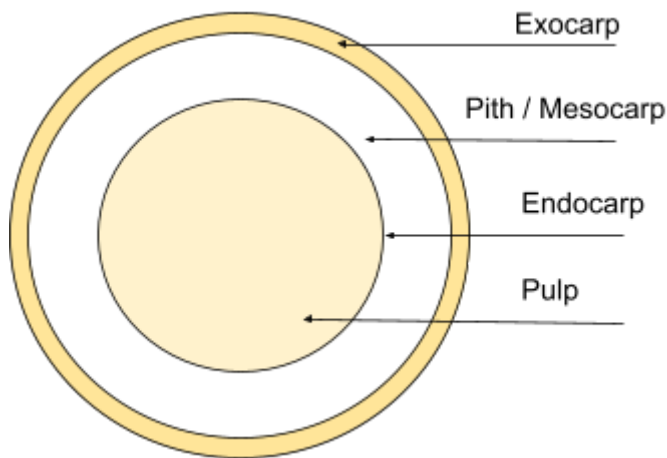


Figure 11: Location of pith in a citrus peel..

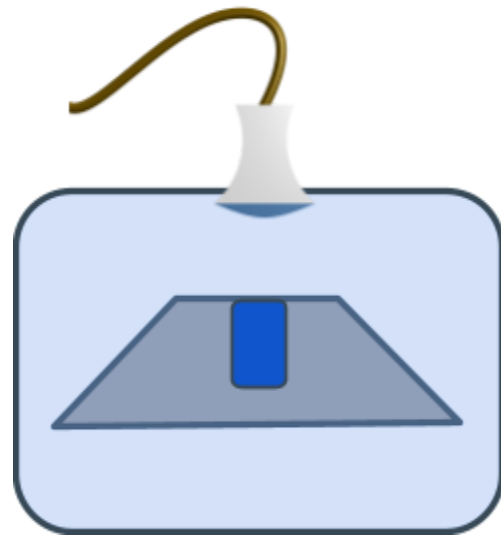


Figure 12: Cross section of Pith Pit model construction.

Model Construction

Components:

- Pomelo Fruit Pith
- Water bath

Procedure:

1. The water bath is degassed.
2. A section of pith at least 3 by 2 cm is isolated from the fruit using a razor blade. It is important that there will not be oil glands left on the peel and that cuts will be made flat because scoring the surface will lead to other artifacts.
3. In the top of the peel a hole is made using a drill bit so that the material is removed while taking care not to bruise the area around the hole.
4. Then the peel is placed in the water bath with the hole facing up.
5. While held at a depth of around 4 cm the model is scanned from above.

Imaging Parameters:

Imaging was conducted using a GE Alton S70 ultrasound research system (GE Healthcare, Chicago, IL, USA) equipped with a 12S phased-array sector probe. These settings were chosen to optimize visualization of potential B-line artifacts while maintaining clinically relevant imaging conditions. The following imaging parameters were used:

- Frequency: 4.5 MHz
- MI of 0.7
- Depth: 10 cm
- Gain: 0 dB
- Dynamic Range: 65 dB
- Focus: Set at the simulated pleural line interface

Experiment: Change diameter of the holes.

In this experiment the length of the vertical artifacts created was compared to the diameter of the hole bored in the peel surface. All holes were made with a constant 2 mm of depth. Hole diameters between 1 and 3 mm were investigated.

6.4 Digital Simulations

Digital simulations of the membrane were conducted to see if it could be transferring energy to sites of B-line formation through Lamb waves. LS-DYNA by Ansys was used to model the propagation of a stimulated impulse in a membrane with material properties similar to those of the visceral pleura as found in the literature [Lu, 2022]. The modeled membrane had a thickness of 100 micrometers, was viscoelastic and was under initial surface tension.

Experiment: Free case

The visceral membrane was modeled with its viscoelastic properties. The membrane was modeled using shell elements with a thickness of 100 micrometers and two square sections of 3 cm by 3 cm which connect at a 45 degree angle from level. The poisson's ratio was set at 0.42 as per Butler (1986).

The simulation starts with a prescribed oscillatory motion applied to a group of nodes from the surface of the simulated membrane and bounded by a circle. The motion used is 2.5 sinusoidal cycles at 1 MHz and an amplitude of 0.5 mm. The boundary conditions along the long edges permit no motion but allow rotation.

The viscoelastic values for the pulmonary visceral pleural membrane are derived from the work in the paper by Lu (2022). From this work the stress-strain curves and relaxation moduli fitted to a Maxwell-Wiechert of bovine pleural membrane were chosen. This experiment does not account for the single sided fluid loading on the visceral pleura or the connections to the parenchyma.

7. Results

7.1 Wrapped Sponge

Experiment: Change the water fraction of the sponge.

Vertical artifacts were seen from the surface at seemingly random locations while at the edges there was occasionally a strong long artifact (Figure 14). These were found to occur where the wrap was loose and touched the gel spacer. With more water, there were more artifacts all of which were short until the sponge took on the appearance of "white lung". The established cut off for long artifacts in this work was set at 4 cm which was slightly greater than the thickness of the sponge.

With more water saturation of the sponge, more artifacts were seen. They got a little longer with increasing water saturation, but they were never longer than 4 cm.

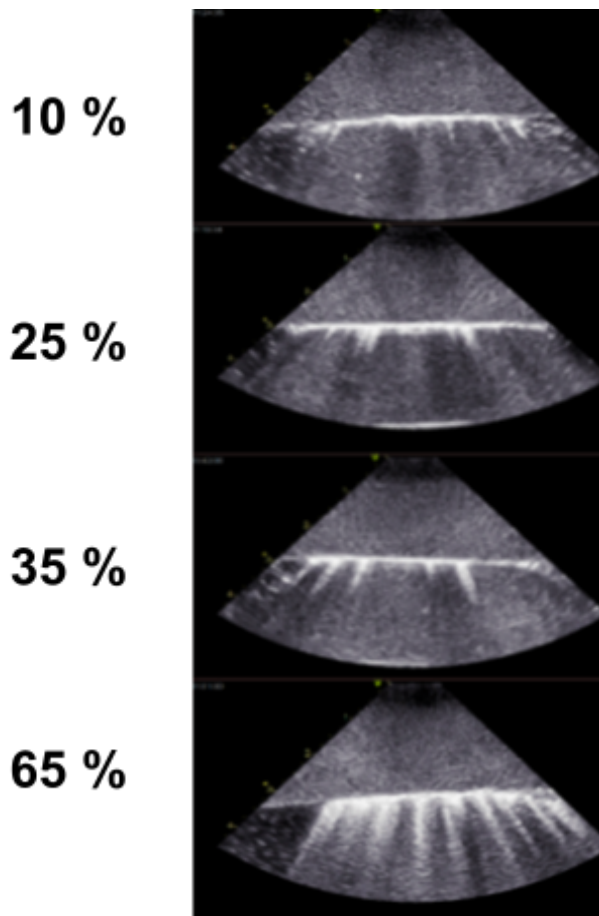


Figure 13: Wrapped Sponge artifacts with increasing saturation.



Figure 14: Ultrasound image of the Wrapped Sponge edge artifact and smaller artifacts at the gel-sponge interface.

7.2 Membrane Vice

Experiment: Change the shape of the fold in the membrane.

Of the types of folds tested, the Concave V-shaped fold was the one that reliably made long vertical artifacts over 4 cm. Where these artifacts appeared they erased the A-lines.

Experiment: Change the Material of the membrane.

No vertical artifacts were seen arising from the vinyl membrane. There were strong artifacts from the other two membranes. All membranes were able to form A-lines but the A-lines were erased when there were long vertical artifacts.



Figure 15: Comparison of artifacts generated by different membrane materials..

Experiment: Using a bag as the membrane. Dry inside.

The bags filled with dry air still created vertical artifacts just as had the membrane sheets.

7.3 Pith Pits

Experiment: Change diameter of the holes.

The width of the holes had no effect on the length of the artifacts that came from holes of the same depth in the range of 1-3 mm. Even smaller holes were tried using a needle head but the exact dimensions were difficult to measure beyond knowing that they are less than 1 mm in diameter. These smallest holes did produce shorter artifacts.

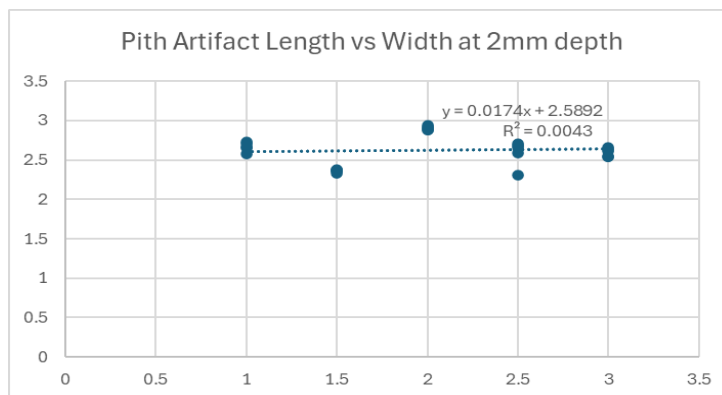


Figure 16: Relationship between pit diameter and artifact length for 2mm deep Pith Pits.

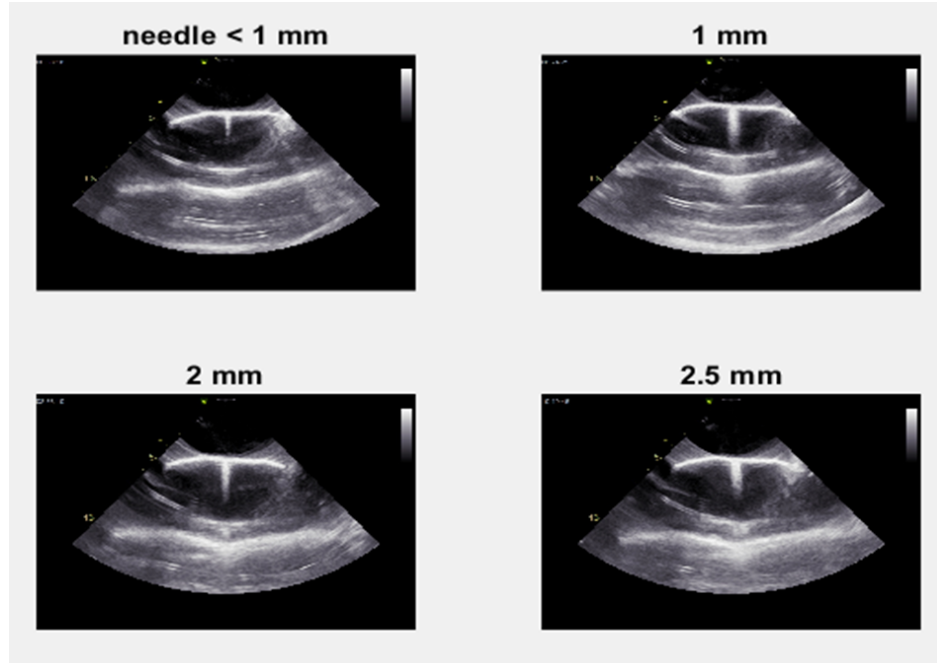


Figure 17: Representative images from the Pith Pit experiments. The pits had different diameters and a constant 2 mm depth.

7.4 Digital Simulation

Experiment: Free Case

Following the prescribed vertical motion stimulus to a portion of the membrane at the beginning of the simulation there was a wave that propagated through the membrane. This wave reached the edge which was 15 mm from the point of the stimulation after around 1.7 ms. The speed of the wave was therefore close to 9 m/s. Despite the viscoelastic nature of the medium the wave did not lose so much energy that it was unable to continue moving through the material and it even followed the bend of the simulated membrane.

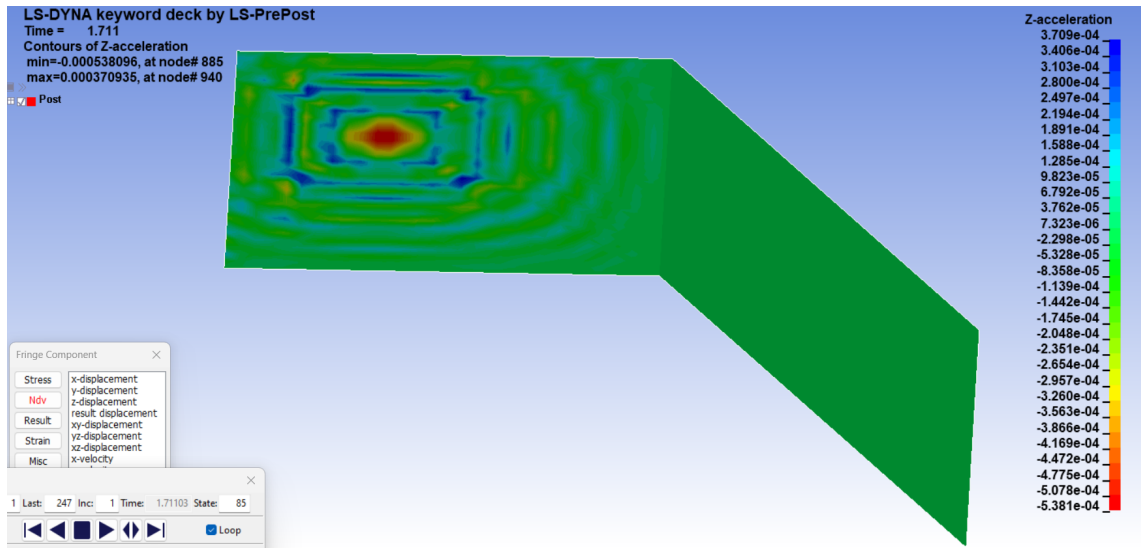


Figure 18: Surface wave in membrane reaches edge.

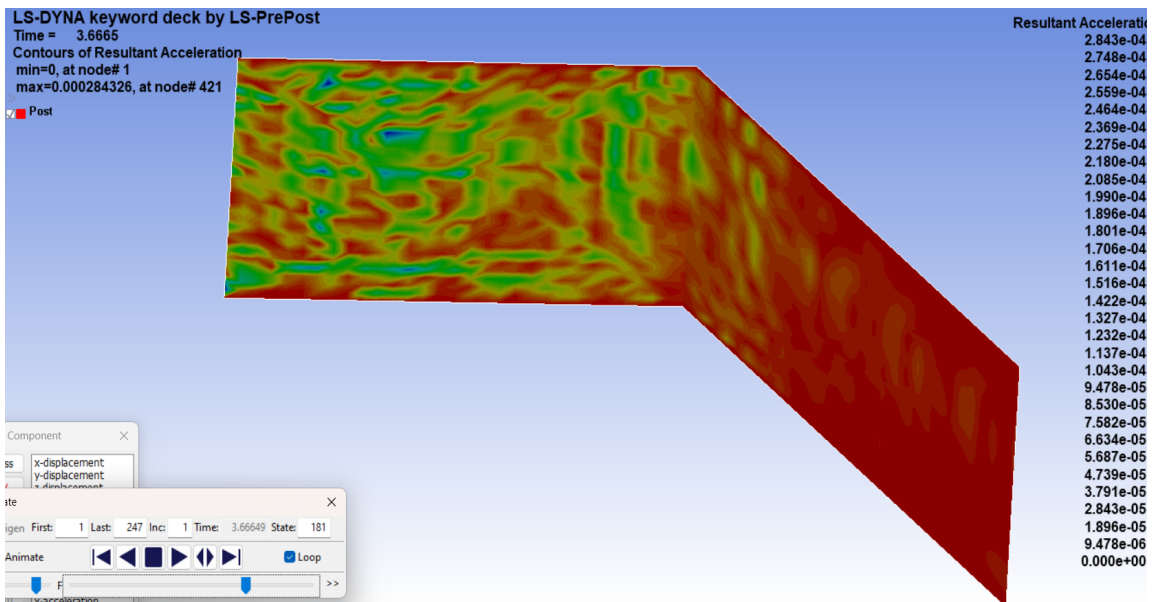


Figure 19: Surface wave in membrane follows the waveguide through the edge.

8. Discussion

This study aimed to investigate the role of the pleural membrane in the formation of B-line artifacts in LUS. It was hypothesized that the pleural membrane is the source of B-lines, and that the reverberation artifact is prolonged by a resupply of energy transferred through surface waves in the pleura. The results from the experimental models provide novel insights into the potential mechanisms underlying B-line generation, with significant implications for both theoretical understanding and clinical practice.

Summary of Key Findings

The Wrapped Sponge model is similar to the naive approach taken by several other studies. It was able to generate short artifacts at the interface of the gel and the wetted sponge. These artifacts increased in number and slightly in size until the sponge took on the appearance of “white lung.” The vertical artifact that best matched B-lines in appearance, however, was actually the unexpected artifact occurring at the edges of the phantom. Long strong vertical artifacts arose where a loose fold of the plastic film covering the sponge made contact with the gel spacer. A recent paper mentioned a similar edge artifact [Demi, 2023], but did not further investigate it.

Conversely, in this work, observing that the membrane alone was sufficient to make strong long vertical artifacts, the next model, the Membrane Vice, was developed. The Membrane Vice model showed that simple concave v-shaped folds in a membrane could consistently produce long vertical artifacts reminiscent of B-lines. This model was also useful in showing how not all materials were equal in their ability to make the vertical artifacts. Some membranes (plastic wrap and sausage casing) produced strong artifacts while others (vinyl rubber) did not. This supports the assertion that vibration in the membrane affects the production of artifacts.

This supposition was further strengthened with the pith experiments. The pith pit was similar to the fold in the membrane; having water surrounded by an air-containing region. It was shown though that without a membrane the pith pit model was not enough to form long artifacts, only short ones. The pith could be prepared with a hole all the way through it and still make short vertical artifacts. This points towards the artifact being a reverberation artifact and that the reverberation is too transient to cause the long artifacts seen with the membrane vice experiments. Alternatively, the impedance change from the water to the pith is less abrupt than that of the membrane, perhaps due to tissue bruising in the walls around the drilled hole. Slower changes in impedance would lead to greater energy losses and potentially a shorter artifact.

The digital simulation provided further support for the proposed theory, demonstrating the feasibility of surface waves propagating along the lung surface despite its viscoelasticity. These waves move quickly enough that they could potentially resupply energy to B-line origin sites, explaining the persistent nature of these artifacts in clinical observations. When the lung gets too full of water the additional fluid loading may greatly attenuate these vibrations and eliminate this lateral energy transfer. While it is true that the anatomy of the pleura has multiple layers for the purpose of this simulation the increase of complexity in the model would not likely be compensated for by improved understanding of the system since the reflections caused by acoustic impedance differences between the individual layers are orders of magnitude small than that of the air-water interface and will not trap a significant amount of waves between them. Furthermore, the physical experiments with the Membrane Vice model showed that vertical artifacts could be replicated with a single membrane.

Comparison with Existing Literature

These findings both complement and challenge existing theories of B-line formation. As noted in the literature review, most existing theories focus on parenchymal explanations for B-line formation. For instance, Avruch and Cooperburg's bubble tetrahedron theory (1985) emphasizes the role of alveolar flooding. While our results do not necessarily contradict previous theories, they suggest that the pleural membrane itself may be capable of generating B-line artifacts without the need for subpleural fluid accumulation. Pleura-genic and parenchyma-genic B-lines may both be present in the diseased lung. Ultimately, it is possible for several mechanisms to be at play. Direct study of ex vivo lungs could prove more definitive.

The digital phantom of Silva (2022) may seem similar to the Membrane Vice experiments due to both having an extension of acoustically permeable material into the air region. However, there are two main differences. First, unlike in Silva it was not necessary to have a large degree of heterogeneity within the infiltrated zone. In this work the infiltrate is just water. Secondly, in this work the A-lines are erased whereas in Silva there was no erasure of A-lines. For these reasons it is not correct to say that this work is solely a physical implementation of the numerical model of Silva.

Theoretical Implications

The novel perspective on B-line formation presented in this study, suggesting a "pleura-genic" mechanism alongside the traditionally considered "parenchyma-genic" explanations may help explain some of the inconsistencies in previous literature and clinical observations.

For example, the erasure of A-lines in the presence of B-lines, a phenomenon noted in early definitions but often unexplained by parenchymal theories, can be readily accounted for by a pleural mechanism. Surface irregularities that generate B-lines could simultaneously disrupt the smooth pleural surface necessary for A-line formation. As has been noted some surface treatments to metal medical apparatus can reduce reverberation artifacts [Huang, 2007]. Aged lungs are also theorized to be less likely to produce A-lines and more likely to produce B-Lines because of scarring acquired over a lifetime [Chiesa, 2014].

Examining the pleura as the source of B-lines can also help to explain why B-lines are seen in some diseases where there is no extra fluid in the lungs like pulmonary fibrosis or in the presence of pleural lesions [Mohammadi, 2014] [Pinal-Fernandez, 2015] [Buda, 2015] [Song, 2016].

Vertical artifacts may be on a spectrum from long to short in the body depending on the level of pleural involvement.

Clinical Implications

The potential clinical implications of this work are significant. If B-line formation is indeed closely tied to the state of the pleural membrane, it opens up new possibilities for the interpretation of LUS findings. B-line characteristics could potentially provide information about pleural properties such as stiffness or thickness, which may be indicative of specific pathological processes. It is also possible that if B-lines indicate the presence of pleural irregularities then mild pleural irregularities are more common than previously thought in COVID19. Many studies have ignored pleural irregularities. The co-occurrence of A-lines and B-lines may be diagnostically significant and signal that the B-lines are not of pleural origin.

Novel Contributions

The membrane vice model represents a vast reduction in model complexity. This opens the doors to more exact experimentation that can easily refer to and modify the ground truth of the experiment. The strong focus on the pleura is also unique in the literature on the physiological explanations of B-lines. This work provides a possible explanation that addresses the often-observed erasure of A-lines in clinical scans where there are B-lines. The membrane vice model creates long vertical artifacts that break A-lines.

Addressing potential criticisms:

One potential criticism of this work is that the pleural membrane may be less distinct than presented, potentially just representing the peripheral section of the interstitium. While this is a valid consideration, it is important to note that under high-frequency ultrasound, the pleura does appear as two distinct lines. The clinical relevance of distinguishing between pleura and interstitium could be questioned, as diseases affecting one may impact the other. However, this work demonstrates that even subtle changes in the pleural membrane can generate B-lines, suggesting its importance as a distinct structure in lung ultrasound interpretation.

Another potential criticism is that if pleural differences are responsible for B-lines, then why aren't these differences directly visible in ultrasound scans? The key point here is that the pleural irregularities generating B-lines may be quite small, potentially below the resolution limit of typical B-mode scans. It is worth noting that pleural irregularities are typically investigated using higher frequencies (around 10 MHz) than those used for B-line analysis (1-5 MHz), which may contribute to the underappreciation of pleural involvement in B-line formation. Moreover, the B-line itself may obscure the view of its originating site. This is consistent with observations from the Membrane Vice model, where small folds produced prominent artifacts. It is also important to consider that routine lung ultrasound protocols may not always include detailed examination of the pleura, and when such examinations are performed, they typically use higher frequencies than those used for B-line analysis. This could lead to an underestimation of the prevalence and significance of minor pleural irregularities. Several studies in the literature have indeed noted the coexistence of pleural lesions and B-lines, supporting the potential link between pleural changes and B-line formation.

As for why the plastic film on the sponge doesn't lead to energy transfer and extension of the vertical artifact at the gel-sponge interface, this can be explained by the fundamental differences between the model and the actual lung anatomy. In the sponge model, the plastic film is not physically connected to or integrated with the sponge structure. It merely serves as an external covering. In contrast, the visceral pleura in the lung is intimately connected to the underlying parenchyma through the thin walls of the alveoli and also under surface tension. The lack of this connection in the sponge model likely prevents the kind of energy transfer and artifact extension observed in the Membrane Vice experiments and hypothesized to occur in actual lungs.

Limitations

The limitations of this study should be acknowledged. Firstly, while the models provided valuable insights, they are an idealization of the true physiology. The experimental models, particularly the Membrane Vice, represent significant simplifications of the complex lung environment. While this simplification allows for focused investigation of specific mechanisms, it may not fully capture all the nuances of *in vivo* B-line formation. The exact acoustic properties of the experimental membranes also likely differ from those of the actual visceral and parietal pleura, potentially affecting the generalizability of these results. The lack of *in vivo* experiments or studies with actual lung tissue limits the direct clinical applicability of our findings.

Secondly, this study did not employ spectrographic analysis of the observed artifacts. Such analysis could have provided more detailed information about the frequency characteristics and modulation patterns of the observed vertical artifacts, potentially offering deeper insights into their formation mechanisms.

The digital simulation of Lamb waves was conducted on a free membrane, whereas the visceral pleura *in vivo* experiences fluid loading on one side and is connected on the other to the lung parenchyma through thin alveolar walls. This simplification may affect the accuracy of the simulated wave propagation. Run times incorporating fluid loading were predicted to take 30 days to run.

9. Conclusions

In conclusion, as opposed to most other works which focus on the parenchyma as the source of B-lines, this study highlights the involvement of the pleura. The Membrane Vice experiments demonstrate that a membrane with irregularities at the interface of a large impedance difference is sufficient to explain the formation of B-lines. Continuing to overlook the pleura's role in lung ultrasound research would be a mistake.

Vertical artifacts formed through this membrane mechanism are affected by the properties of the membrane. The stiffness and folding behavior of the membrane can completely impede B-line formation.

This work supports the assertion that even mild pleural irregularity can lead to the formation of B-lines.

The developed phantom can accurately replicate vertical artifacts, not only for advancing our understanding but also for training ultrasound technicians and improving the collection of clinically relevant images. The effects of a thin membrane must be considered in phantom design as these can generate artifacts on their own.

Although the evidence supporting Lamb wave transmission in this context remains limited, further investigation into these physical processes during disease development could significantly enhance our comprehension of lung pathology progression. Ultimately, this work underscores the need for a more comprehensive approach to understanding B-line formation, integrating both pleural and parenchymal factors to improve the diagnostic capabilities of lung ultrasound.

10. Bibliography

1. Ansys® Academic Research LS-DYNA PrePost, Release 4.10
2. Adams HJA, Kwee TC, Yakar D, Hope MD, Kwee RM. Chest CT Imaging Signature of Coronavirus Disease 2019 Infection. *Chest*. 2020;158(5):1885-1895. doi: 10.1016/j.chest.2020.06.025
3. Alrajab S, Youssef AM, Akkus NI, Caldito G. Pleural ultrasonography versus chest radiography for the diagnosis of pneumothorax: review of the literature and meta-analysis. *Critical Care*. 2013;17(5):R208. doi: 10.1186/cc13016
4. Avruch L, Cooperberg PL. The ring-down artifact. *J Ultrasound Med*. 1985;4(1):21-28. Doi: 10.7863/jum.1985.4.1.21
5. Azhari H, Kennedy JA, Weiss N, Volokh L. From Signals to Image: A Basic Course on Medical Imaging for Engineers. *Springer*. 2020.
6. Bhoil R, Ahluwalia A, Chopra R, Surya M, Bhoil S. Signs and lines in lung ultrasound. *J Ultrason*. 2021;21(86):e225-e233. doi: 10.15557/jou.2021.0036
7. Blanco PA, Cianciulli TF. Pulmonary Edema Assessed by Ultrasound: Impact in Cardiology and Intensive Care Practice. *Echocardiography*. 2016;33(5):778-787. doi: 10.1111/echo.13182
8. Blüthgen C, Sanabria S, Frauenfelder T, Klingmüller V, Rominger M. Economical Sponge Phantom for Teaching, Understanding, and Researching A- and B-Line Reverberation Artifacts in Lung Ultrasound. *J Ultrasound Med*. 2017;36(10):2133-2142. doi: 10.1002/jum.14266
9. Buda N, Piskunowicz M, Porzezińska M, Kosiak W, Zdrojewski Z. Lung Ultrasonography in the Evaluation of Interstitial Lung Disease in Systemic Connective Tissue Diseases: Criteria and Severity of Pulmonary Fibrosis – Analysis of 52 Patients. *Ultraschall Med*. 2015;37(4):379-385. doi: 10.1055/s-0041-110590
10. Buda N, Skoczylas A, Demi M, Wojteczek A, Cylwik J, Soldati G. Clinical Impact of Vertical Artifacts Changing with Frequency in Lung Ultrasound. *Diagnostics (Basel)*. 2021;11(3):401. doi: 10.3390/diagnostics11030401
11. Butler JP, Nakamura M, Sasaki H, Sasaki T, Tamotsu Takishima. Poissons' ratio of lung parenchyma and parenchymal interaction with bronchi. *Jpn J Physiol*. 1986;36(1):91-106. doi: 10.2170/jjphysiol.36.91

12. Chiesa AM, Ciccarese F, Gardelli G, et al. Sonography of the normal lung: Comparison between young and elderly subjects. *J Clin Ultrasound*. 2014;43(4):230-234. doi: 10.1002/jcu.22225
13. Chua MT, Boon Y, Yeoh CK, Li Z, Goh CJM, Kuan WS. Point-of-care ultrasound use in COVID-19: a narrative review. *Ann Transl Med*. 2024;12(1):13-13. doi: 10.21037/atm-23-1403
14. Ciurba BE, Sárközi HK, Szabó IA, et al. Applicability of lung ultrasound in the assessment of COVID-19 pneumonia: Diagnostic accuracy and clinical correlations. *Respir Investig*. 2022;60(6). doi: 10.1016/j.resinv.2022.06.015
15. COMSOL Multiphysics® www.comsol.com. COMSOL AB, Stockholm, Sweden.
16. Copetti R, Soldati G, Copetti P. Chest sonography: a useful tool to differentiate acute cardiogenic pulmonary edema from acute respiratory distress syndrome. *Cardiovasc Ultrasound*. 2008;6(1). doi: 10.1186/1476-7120-6-16
17. Demi M. On the Replica of US Pulmonary Artifacts by Means of Physical Models. *Diagnostics (Basel)*. 2021;11(9):1666. doi: 10.3390/diagnostics11091666
18. Demi M, Buda N, Soldati G. Vertical Artifacts in Lung Ultrasonography: Some Common Clinician Questions and the Related Engineer Answers. *Diagnostics (Basel)*. 2022a;12(1):215. doi: 10.3390/diagnostics12010215
19. Demi L, Demi M, Prediletto R, Soldati G. Real-time multi-frequency ultrasound imaging for quantitative lung ultrasound – first clinical results. *J Acoust Soc Am*. 2020a;148(2):998-1006. doi: 10.1121/10.0001723
20. Demi M, R. Prediletto, Soldati G, Demi L. Physical Mechanisms Providing Clinical Information From Ultrasound Lung Images: Hypotheses and Early Confirmations. *IEEE Trans Ultrason Ferroelectr Freq Control*. 2020b;67(3):612-623. doi: 10.1109/tuffc.2019.2949597
21. Demi M, Soldati G, Demi L. On the artefactual information of ultrasound lung images: A lines and B lines. *Proc Meet Acoust*. 2018;35(1). doi: 10.1121/2.0000943
22. Demi M, Soldati G, Ramalli A. Lung Ultrasound Artifacts Interpreted as Pathology Footprints. *Diagnostics (Basel)*. 2023;13(6):1139. doi: 10.3390/diagnostics13061139
23. Demi L, Wolfram F, Klerys C, et al. New International Guidelines and Consensus on the Use of Lung Ultrasound. *J Ultrasound in Med*. 2022b;42(2). doi: 10.1002/jum.16088
24. Demi L, van Hoeve W, van Sloun RJG, Soldati G, Demi M. Determination of a potential quantitative measure of the state of the lung using lung ultrasound spectroscopy. *Sci Rep*. 2017;7(1). doi: 10.1038/s41598-017-13078-9

25. Duck FA. Hazards, risks and safety of diagnostic ultrasound. *Med Eng Phys*. 2008;30(10):1338-1348. doi: 10.1016/j.medengphy.2008.06.002
26. Esclar JD, Esclar A. Lung hysteresis: a morphological view. *Histol Histopathol*. 2004;19(1):159-166. doi: 10.14670/HH-19.159
27. Gargani L, Doveri M, D'Errico L, et al. Ultrasound lung comets in systemic sclerosis: a chest sonography hallmark of pulmonary interstitial fibrosis. *Rheumatology (Oxford)*. 2009;48(11):1382-1387. doi: 10.1093/rheumatology/kep263
28. Gill RR, Gerbaudo VH, Jacobson FL, et al. MR Imaging of Benign and Malignant Pleural Disease. *Magn Reson Imaging Clin N Am*. 2008;16(2):319-339. doi: 10.1016/j.mric.2008.03.004
29. Harrison BP, Crystal CS. Imaging modalities in obstetrics and gynecology. *Emerg Med Clin North Am*. 2003;21(3):711-735. doi:10.1016/s0733-8627(03)00047-6
30. Haurylenka D, Damantsevich V, Filustsin A, Damantsevich A. Diagnostic value of 12-zone lung ultrasound protocol for diagnosing COVID-19-associated pneumonia in outpatients. *J Ultrason*. 2021;21(87):e271-e276. doi:10.15557/JoU.2021.0046
31. Herbst MK, Velasquez J, Adnan G, O'Rourke MC. Cardiac Ultrasound. In: StatPearls. Treasure Island (FL): StatPearls Publishing; November 21, 2022.
32. Huang J, Triedman JK, Vasilyev NV, Suematsu Y, Cleveland RO, Dupont PE. Imaging Artifacts of Medical Instruments in Ultrasound-Guided Interventions. *J Ultrasound Med*. 2007;26(10):1303-1322. doi: 10.7863/jum.2007.26.10.1303
33. Jambrik Z, Monti S, Coppola V, et al. Usefulness of ultrasound lung comets as a nonradiologic sign of extravascular lung water. *Am J Cardiol*. 2004;93(10):1265-1270. doi: 10.1016/j.amjcard.2004.02.012
34. Kameda T, Kamiyama N, Taniguchi N. The Mechanisms Underlying Vertical Artifacts in Lung Ultrasound and Their Proper Utilization for the Evaluation of Cardiogenic Pulmonary Edema. *Diagnostics (Basel)*. 2022;12(2):252. doi: 10.3390/diagnostics12020252
35. Kameda T, Kamiyama N, Taniguchi N. Simple Experimental Models for Elucidating the Mechanism Underlying Vertical Artifacts in Lung Ultrasound: Tools for Revisiting B-Lines. *Ultrasound Med Biol*. 2021;47(12):3543-3555. doi: 10.1016/j.ultrasmedbio.2021.08.019
36. Kameda T, Taniguchi N, Konno K, et al. Ultrasonography in undergraduate medical education: a comprehensive review and the education program implemented at Jichi Medical University. *J Med Ultrasonics*. 2022;49:217-230. doi: 10.1007/s10396-021-01178-z

37. Leote J, Tiago Muxagata, Guerreiro D, et al. Influence of Ultrasound Settings on Laboratory Vertical Artifacts. *Ultrasound Med Biol.* 2023;49(8):1901-1908. doi: 10.1016/j.ultrasmedbio.2023.03.018
38. Lichtenstein DA. Lung ultrasound in the critically ill. *Ann Intensive Care.* 2014;4(1):1. Published 2014 Jan 9. doi: 10.1186/2110-5820-4-1
39. Lichtenstein DA, Lascols N, Prin S, Mezière G. The “lung pulse”: an early ultrasound sign of complete atelectasis. *Intensive Care Med.* 2003;29(12):2187-2192. doi: 10.1007/s00134-003-1930-9
40. Lichtenstein DA, Mezière GA. Relevance of Lung Ultrasound in the Diagnosis of Acute Respiratory Failure*: The BLUE Protocol. *Chest.* 2008;134(1):117-125. doi: 10.1378/chest.07-2800
41. Lichtenstein D, Mezière G. A lung ultrasound sign allowing bedside distinction between pulmonary edema and COPD: the comet-tail artifact. *Intensive Care Med.* 1998;24(12):1331-1334. doi: 10.1007/s001340050771
42. Lichtenstein D, Mézière G, Biderman P, Gepner A, Barré O. The comet-tail artifact. An ultrasound sign of alveolar-interstitial syndrome. *Am J Respir Crit Care Med.* 1997;156(5):1640-1646. doi:10.1164/ajrccm.156.5.96-07096
43. Lin H, Zhang B, Kou H, et al. Application value of lung ultrasound in asymptomatic patients with confirmed COVID-19. *Advanced Ultrasound in Diagnosis and Therapy.* 2020;4(2):67-72. doi: 10.37015/AUDT.2020.200025
44. Lopes AJ, Mafort TT, Costa CH, et al. Comparison Between Lung Ultrasound and Computed Tomographic Findings in Patients With COVID - 19 Pneumonia. *J Ultrasound Med.* 2020;40(7):1391-1399. doi: 10.1002/jum.15521
45. Lu X, Han L, Kassab GS. Pulmonary Visceral Pleura Biomaterial: Elastin- and Collagen-Based Extracellular Matrix. *Front Bioeng Biotechnol.* 2022;10:796076. doi:10.3389/fbioe.2022.796076
46. Manolescu D, Davidescu L, Traila D, Oancea C, Tudorache V. The reliability of lung ultrasound in assessment of idiopathic pulmonary fibrosis. *Clin Interv Aging.* 2018;13:437-449. doi:10.2147/CIA.S156615
47. Marchetti G, Arondi S, Baglivo F, et al. New insights in the use of pleural ultrasonography for diagnosis and treatment of pleural disease. *Clin Respir J.* 2018;12(6):1993-2005. doi:10.1111/crj.12907
48. Marini TJ, Rubens DJ, Zhao YT, et al. Lung Ultrasound: The Essentials. *Radioi Cardiothorac Imaging.* 2021;3(2):e200564. Published 2021 Apr 29. doi:10.1148/ryct.2021200564

49. Mathis G, Horn R, Morf S, et al. WFUMB position paper on reverberation artefacts in lung ultrasound: B-lines or comet-tails?. *Med Ultrason.* 2021;23(1):70-73. doi:10.11152/mu-2944
50. Mento F, Khan U, Faita F, et al. State of the Art in Lung Ultrasound, Shifting from Qualitative to Quantitative Analyses. *Ultrasound Med Biol.* 2022;48(12):2398-2416. doi: 10.1016/j.ultrasmedbio.2022.07.007
51. Miller DL, Dou C, Dong Z. Lung Ultrasound Induction of Pulmonary Capillary Hemorrhage in Neonatal Swine. *Ultrasound Med Biol.* 2022;48(11):2276-2291. doi: 10.1016/j.ultrasmedbio.2022.06.020
52. Mohammadi A, Oshnoei S, Ghasemi-rad M. Comparison of a new, modified lung ultrasonography technique with high-resolution CT in the diagnosis of the alveolo-interstitial syndrome of systemic scleroderma. *Med Ultrason.* 2014;16(1):27-31. doi: 10.11152/mu.2014.2066.161.am1so2
53. Morgan RA, Pickworth FE, Dubbins PA, McGavin CR. The ultrasound appearance of asbestos-related pleural plaques. *Clin Radiol.* 1991;44(6):413-416. doi: 10.1016/s0009-9260(05)80662-2
54. Moyano DB, Paraiso DA, González-Lezcano RA. Possible Effects on Health of Ultrasound Exposure, Risk Factors in the Work Environment and Occupational Safety Review. *Healthcare (Basel).* 2022;10(3):423. doi: 10.3390/healthcare10030423
55. Park EJ, Yoon YT, Hong CK, Ha YR, Ahn JH. Randomized, noninferiority study between video versus hand ultrasound with wet foam dressing materials to simulate B-lines in lung ultrasound: A CONSORT-compliant article. *Medicine (Baltimore).* 2017;96(30):e7642. doi: 10.1097/MD.00000000000007642
56. Pinal-Fernandez I, Pallisa-Nuñez E, Selva-O'Callaghan A, et al. Pleural irregularity, a new ultrasound sign for the study of interstitial lung disease in systemic sclerosis and antisynthetase syndrome. *Clin Exp Rheumatol.* 2015;33(4 Suppl 91):S136-S141
57. Łyżniak P, Świętoń D, Serafin Z, Szurowska E. Lung ultrasound in a nutshell. Lines, signs, some applications, and misconceptions from a radiologist's point of view. *Pol J Radiol.* 2023;88:294-310. doi: 10.5114/pjr.2023.128866
58. Rose JL. Ultrasonic Guided Waves in Solid Media. Cambridge University Press; 2014.
59. Safai Zadeh E, Görg C, Prosch H, et al. Lung ultrasound and pleural artifacts: A pictorial review. *Diagnostics.* 2024;14(2):179. doi: 10.3390/diagnostics14020179
60. Saha BK, Chong WH, Austin A, et al. Pleural abnormalities in COVID-19: a narrative review. *J Thorac Dis.* 2021;13(7):4484-4499. doi: 10.21037/jtd-21-542

61. Silva FAMD, Moreno E, Pereira WCA. B-Lines Lung ultrasonography simulation using finite element method. *Diagnostics (Basel)*. 2022;12(11):2751. doi: 10.3390/diagnostics12112751
62. Smargiassi A, Zanforlin A, Perrone T, et al. Vertical Artifacts as Lung Ultrasound Signs: Trick or Trap? Part 2- An Accademia di Ecografia Toracica Position Paper on B-Lines and Sonographic Interstitial Syndrome. *J Ultrasound Med.* 2023;42(2):279-292. doi:10.1002/jum.16116
63. Soldati G, Copetti R, Sher S. Sonographic Interstitial Syndrome. *J Ultrasound Med.* 2009;28(2):163-174. doi: 10.7863/jum.2009.28.2.163
64. Soldati G, Demi M. The use of lung ultrasound images for the differential diagnosis of pulmonary and cardiac interstitial pathology. *J Ultrasound*. 2017;20(2):91-96. Published 2017 Apr 7. doi: 10.1007/s40477-017-0244-7
65. Soldati G, Demi M, Inchincolo R, Smargiassi A, Demi L. On the physical basis of pulmonary sonographic interstitial syndrome. *J Ultrasound Med.* 2016;35(10):2075-2086. doi: 10.7863/ultra.15.08023
66. Soldati G, Giunta V, Sher S, Melosi F, Dini C. "Synthetic" Comets: A New Look at Lung Sonography. *Ultrasound Med Biol.* 2011;37(11):1762-1770. doi: 10.1016/j.ultrasmedbio.2011.05.024
67. Soldati G, Inchincolo R, Smargiassi A, et al. Ex vivo lung sonography: morphologic-ultrasound relationship. *Ultrasound Med Biol.* 2012;38(7):1169-1179. doi:10.1016/j.ultrasmedbio.2012.03.001
68. Soldati G, Smargiassi A, Inchincolo R, et al. Proposal for international standardization of the use of lung ultrasound for patients with COVID-19: A simple, quantitative, reproducible method. *J Ultrasound Med.* 2020;39(7):1413-1419. doi: 10.1002/jum.15285
69. Soldati G, Testa A, Silva FR, Carbone L, Portale G, Silveri NG. Chest ultrasonography in lung contusion. *Chest.* 2006;130(2):533-538. doi:10.1378/chest.130.2.533
70. Sperandeo M, Varriale A, Sperandeo G, et al. Assessment of ultrasound acoustic artifacts in patients with acute dyspnea: a multicenter study. *Acta Radiol.* doi: 10.1258/ar.2012.120340
71. Stone MB, Secko MA. Bedside ultrasound diagnosis of pulmonary contusion. *Pediatr Emerg Care.* 2009;25(12):854-855. doi: 10.1097/PEC.0b013e3181c39a0c
72. Tchelepi H, Ralls PW. Color comet-tail artifact: clinical applications. *AJR Am J Roentgenol.* 2009;192(1):11-18. doi: 10.2214/AJR.07.3893

73. Treeby BE, Cox BT. k-Wave: MATLAB toolbox for the simulation and reconstruction of photoacoustic wave fields. *J Biomed Opt.* 2010;15(2):021314. doi:10.1117/1.3360308
74. Tung-Chen Y, Martí de Gracia M, Díez-Tascón A, et al. Correlation between chest computed tomography and lung ultrasonography in patients with coronavirus disease 2019 (COVID-19). *Ultrasound Med Biol.* 2020;46(11):2918-2926. doi:10.1016/j.ultrasmedbio.2020.07.003
75. Vetrugno L, Baciarello M, Bignami E, et al. The “pandemic” increase in lung ultrasound use in response to Covid-19: Can we complement computed tomography findings? A narrative review. *Ultrasound J.* 2020;12(1):39. doi: 10.1186/s13089-020-00185-4
76. Volpicelli G, Elbarbary M, Blaivas M, et al. International evidence-based recommendations for point-of-care lung ultrasound. *Intensive Care Med.* 2012;38(4):577-591. doi: 10.1007/s00134-012-2513-4
77. Volpicelli G, Frascisco MF. Sonographic detection of radio-occult interstitial lung involvement in measles pneumonitis. *Am J Emerg Med.* 2009;27(1):128.e1-128.e3. doi: 10.1016/j.ajem.2008.03.052
78. Volpicelli G, Lamorte A, Villén T. What's new in lung ultrasound during the COVID-19 pandemic. *Intensive Care Med.* 2020;46(7):1445-1448. doi: 10.1007/s00134-020-06048-9
79. Volpicelli G, Rovida S. Clinical research on point-of-care lung ultrasound: misconceptions and limitations. *Ultrasound J.* 2024;16(1):28. doi: 10.1186/s13089-024-00368-3
80. Wang M, Luo X, Wang L, et al. A Comparison of lung ultrasound and computed tomography in the diagnosis of patients with COVID-19: A systematic review and meta-analysis. *Diagnostics (Basel).* 2021;11(8):1351. doi: 10.3390/diagnostics11081351
81. Wang Y, Zhang Y, He Q, Liao H, Luo J. Quantitative Analysis of Pleural Line and B-Lines in Lung Ultrasound Images for Severity Assessment of COVID-19 Pneumonia. *IEEE Trans Ultrason Ferroelectr Freq Control.* 2022;69(1):73-83. doi:10.1109/TUFFC.2021.3107598
82. Weinberger S, Drazen J. Diagnostic Procedures in Respiratory Disease. In: E Braunwald E, Fauci AS, Hauser SL, Jameson JL, Kasper DL, Longo DL eds. *Harrison's Principles of Internal Medicine.* 16th ed. McGraw-Hill; 2005:1505-1508. doi: 10.1036/0071402357
83. Wu H, Zhang B, Li J, Liu Q, Zhao T. Echogenic foci with comet-tail artifact in resected thyroid nodules: Not an absolute predictor of benign disease. *PLOS ONE.* 2018;13(1):e0191505-e0191505. doi: 10.1371/journal.pone.0191505
84. Yue Lee FC, Jenssen C, Dietrich CF. A common misunderstanding in lung ultrasound: the comet tail artefact. *Med Ultrason.* 2018;20(3):379. doi: 10.11152/mu-1573

**Begetting B-lines: On the Involvement of the Pleural Membrane in the
Physiological Origin of the B-line Artifact**

**Research Thesis
In Partial Fulfillment of The Requirements for the Degree of Master of Science in
Biomedical Engineering**

Aharon Tzvi Verschleisser

**Submitted to the Senate of the Technion - Israel Institute of Technology
Tammuz, 5784 Haifa, July, 2024**

The Research Thesis was done in the Faculty of Biomedical Engineering under the supervision of Prof. Dan Adam

The author of this thesis states that the research, including the collection, processing and presentation of data, addressing and comparing to previous research, etc., was done entirely in an honest way, as expected from scientific research that is conducted according to the ethical standards of the academic world. Also, reporting the research and its results in this thesis was done in an honest and complete manner, according to the same standards.

Acknowledgments

With gratitude to the Lady Davis Scholarship foundation.

יצירת קווי B: על מעורבות קרום הפלאורי במקור הפיזיולוגי של קווי B

חיבור על מחקר

לשם מילוי תפקידו של הדרישות לקבלת התואר מגיסטר למדעים בהנדסה ביו ורפואית

אהרון צבי וורשליניסר

הוגש לסנט הטכניון - מכון טכנולוגי לישראל

תמוז תשפ"ד חיפה, יולי 2024

המחקר נעשה בפקולטה להנדסה ביופרואית בהנחיית פרופ. דן אדם.

מחברת חיבור זה מצהיר/ה כי המחבר, כולל איסוף הנתונים, עיבודם והצגתם, התייחסות והשווואה למחקרים קודמים וכו', נעשה כלו בצורה ישירה, כמצופה מחקר מדעי המבוצע לפי אמות המידה האתניות של העולם האקדמי. כמו כן, הדיווח על המחבר ותוצאותיו בחיבור זה נעשה בצורה ישירה ומלאה, לפי אותן אמות מידה.

אני מודה מאוד לך על הנדיבותה ועל המלגה שהעניקה לי.

תקציר

הכאוס שנגרם עקב התפשטות נגיף תסמנות הנשימה החמורה-2 (SARS-CoV-2) CoronaVirus-2 וחותם האפשרות להביא חולים אלו למכשורי-CT – גרמו לכך שבמספר רב של מקרים דימות אולטרסאונד ריאות (LUS) הפך לכלי מועדף לאבחן, לדרוג החומרה ולניהול המחלת. המגיפה העולמית והכמות האדירה של חולי-19 COVID הדגישה את היתרונות הרבים של שימוש ב-LUS, וזריזו את האימוץ הנרחבותה – בעוד שדיווחים על שימוש ב-LUS פורסמו כבר בשנות ה-60. למורת שהפטנציאל של LUS הוכר בקרב חוקרים במשך עשרות שנים, האימוץ הקליני מאד התעכב עקב העדר מידע מבני, שלא קיים בסריקות ריאות. אך עם פרוץ המגיפה, השיטות שפותחו לאבחן, דרגוג החומרה וניהול סיכונים של חולים עם COVID-19 הדגימו בבירור את התועלת האמיתית של LUS. זאת בנוסף ליתרונות המשמעותיים של אולטרסאונד רפואי – בבטיחות, עלות נמוכה, דימות בזמן אמיתי ובקצב רכישה מאד מהיר.

התמונהות והסרטונים של ריאות של אדם בריא, המלאות באוויר ולכך מחזירות את כל האנרגיה האולטרסונית – נראות שחורות, כאשר בנוסף מופיעים קווים מקבילים (הנקראים A-lines) לקו הבהיר המתקבל מהדי המمبرנה הפלואורית (המברינה העוטפת את הריאות), ובמרחקים אחידים זה מזה, והזהים למרחק שבין המתפרק לקו הפלואורה. תമונות אלו מוגדרות כדרגת חומרה 0 (Grade 0).

התמונהות והסרטונים של ריאות של חולי-19 COVID חולקו ל-3 דרגות חומרה:
1. Grade 1 – דרגת חומרה קללה-בינונית – התמונהות מכילות 2-3 קוו B
2. Grade 2 – דרגת חומרה קשה – התמונהות מכילות קוו B בשטח <50% מהמיירוח הבין-צילע
3. Grade 3 – דרגת חומרה מאד קשה – התמונהות מכילות אזורים דמווי איברים (Consolidations).

רוב רובם של החולים שางינו לבתי החולים היו בדרגות חומרה 1 וגם 2. لكن גורם מרכזי באבחן באמצעות ה-LUS הם קוו B, קווים (עבים) אנכיים היפר-אקוויים וארכיים עד לסוף האזוז הנסרק בתמונה האולטרסאונד. הנוכחות והכמות של קוו B הפכו לאינדיקטורים מכריעים לקביעת חומרה מחלת-19 COVID ולמיעקב אחר התקדמותה. קיימן אמן קשר בין מספר/עובי קוו B לבין פתולוגיות ריאתית שונה, ובמיוחד במחלת ה-COVID-19, אך הקשר כלל אitem מובן וברור – כיוון שהקו ה-B הנם ארטיפקטים – ואינם הדמים המדמים איבר אמיתי.

אם מנ ארטיפקטים מצויים בתמונהות וסרטוי אולטרסאונד גם של אברים אחרים (לב, כבד, וכו'), אך כמעט תמיד ניתן לזהות את האבר. על פי רוב ארטיפקטים אינם רצויים, וקיימות בספרות שיטות רבות לשינון והפרתאה של ארטיפקטים (ורעים) – הן באולטרסאונד והן בסוגי דימות אחרים. אך באולטרסאונד ריאות (LUS) הם חיוניים ומאפשרים אבחן ודרוג החומרה – כך שההנחה היא כי יש בהם מידע פיזיולוגי/פטולוגי לגבי המטופל.

כאמור, קוו B הם הארטיפקטים החשובים ביותר באולטרסאונד של הריאות. הם מוגדר כקווים אנכיים בתמונה שמתחלים מהפלואורה ומשתרעים עד קצה הצג. ישנן עדויות להופעת קוו B בסוג רב של מחלות ריאה – גם כשים מים בראות וגם כשייש פיברוזיס. המנגנון שמייצר אותם לחלוטין לא ידוע, אך

רוב התיאorias לגבי יצירת קווי B מתמקדות בהסברים פרנסימליים ומצנחות את התקף הפטנציאלי של הפלואורה עצמה.

מחקר זה בוחן את התרומה של קרום הפלואורה לייצור קווי B. במחקר זה, אנו משערם ששינויים גיאומטריים קטנים בפני השטח של הקרום הפלואורי, יוצרים מקורות נקודתיים הפלוטים בחזרה אנרגיה אולטרסונית, וכי קרום הפלואורה עשוי להאריך את אותן קווי B באמצעות העברת הדרגתית של גלי Lamb הנעים בפני השטח של קרום הפלואורה - אל המיקומות בהם קיימים השינויים הגיאומטריים. כדי לבדוק השערות אלו פותחו שלושה מודלים ניסיוניים (פנטומים):

- מודל ספג עטוף
- מודל תפס מمبرנה (membrane vice)
- מודל Pit Pith עשוי מקליפה של פולימר.

סימולציות נומריות באמצעות תוכנת LS-DYNA תשלימו את הניסויים הפיזיים.

מודל הספג העטוף יצר ארטיפקטים ארכיים קצריים שהתארכו קצר עם גידול בתכולת המים בספג. באופן בלתי צפוי, ארטיפקטים ארכיים ארוכים הדומים לקווי B נצפו בקצבות הפנטום שביהם כפל קרום רופפים יצרו מגע עם מרוח הגאל.

המודל של Membrane Vice שבו נמתחה מمبرנה מעלה בעות אויר ומים, מאפשר מתן הסבר/הוכחה לתפקידו של קרום הפלואורה לייצור קווי ה-B. מודל זה מאפשר הוכחה ניסوية שקפלים קעורים פשוטים בצורת V בمبرנה יכולים לייצר באופן עקב ארטיפקטים ארכיים המזכירים קווי B. תכונות החומר של המمبرנה השפיעו באופן שימושו על הייצור ארטיפקטים, כאשר עטיפות פלסטיים ומעטפת נקניק יצרו ארטיפקטים חזקים ואילו מمبرנה עשויות מגומי וויניל לא יצרו ארטיפקטים.

מודל ה-Pit Pith, לעומת זאת, ללא מمبرנה, יצר רק ארטיפקטים קצריים.

הדמיות הדיגיטליות סיפקו תמייה נוספת לניסוי לתיאוריה המוצעת, והדגימו את היכנותם של גלי פני השטח להתפשט לאורך פני השטח המمبرנה ב מהירות מסוימת כדי לספק אנרגיה לאטרים (אי-רציפות) שייצרו את ה-e-hōn-i-B.

ממצאים אלו מצביעים על אפשרות קיום מגנן הקשור לפלאורה שמאפשר הייצור קווי B, לעומת הסבירים קודמים למגנן הקשור לפרנסימה. פרספקטיבה חדשה זו עשויה לשיעם בהסביר תכיפות קליניות כגון מחיקת קווי A בנוכחות קווי B והייצור של קווי B במצבים ללא נזול בריאות. המחקר מرمץ כי מאפייני קווי B יכולים לספק מידע על תכונות פלאורליות, ולפתח אפשרויות חדשות ליישום אולטרסאונד רפואיות.

List of Figures

Figure 1: The anatomical layers encountered in lung ultrasound.	10
Figure 2: An <i>in vitro</i> metal foreign-body artifact.	16
Figure 3: An <i>in vitro</i> glass foreign-body artifact with modulation.	17
Figure 4: 3D model of Avruch's bubble tetrahedron.	23
Figure 5: Experimental replication of Avruch's "Ring Down Artifact."	23
Figure 6: Wrapped Sponge model construction.	29
Figure 7: Conceptual simplification of the Membrane Vice model.	32
Figure 8: 3D CAD design of the Membrane Vice.	33
Figure 9: Membrane Vice experimental setup.	33
Figure 10: Membrane fold geometries in the Membrane Vice.	35
Figure 11: Location of pith in a citrus peel.	36
Figure 12: Cross section of Pith Pit model construction.	36
Figure 13: Wrapped Sponge artifacts with increasing saturation.	39
Figure 14: Ultrasound image of the Wrapped Sponge edge artifact and smaller artifacts at the gel-sponge interface.	40
Figure 15: Comparison of artifacts generated by different membrane materials.	41
Figure 16: Relationship between pit diameter and artifact length for 2mm deep Pith Pits.	41
Figure 17: Representative images from the Pith Pit experiments. The pits had different diameters and a constant 2 mm depth.	42
Figure 18: Surface wave in membrane reaches edge.	43
Figure 19: Surface wave in membrane follows the waveguide through the edge.	43

